Gondwana break-up related magmatism in the Falkland Islands

M. J. Hole[1], R.M. Ellam[2], D.I.M. MacDonald[1] & S.P. Kelley[3]

[1]Department of Geology & Petroleum Geology University of Aberdeen, AB24 3UE, UK
[2] Scottish Universities Environment Research Centre, East Kilbride, Glasgow, G75 0QU, UK
[3] Department of Earth & Environmental Sciences, Open University, Milton Keynes, MK7 6AA UK

Jurassic dykes (c. 182 Ma) are widespread across the Falkland Islands and exhibit considerable geochemical variability. Orthopyroxene-bearing NW-SE oriented quartz-tholeiite dykes underwent fractional crystallization > 1 GPa, and major element constraints suggest that they were derived by melting of pyroxenite-rich source. They have εNd_{182} in the range -6 to -11 and $^{87}Sr/^{86}Sr_{182}$ >0.710 and therefore require an old lithospheric component in their source. A suite of basaltic-andesites and andesites exhibit geochemical compositions transitional between Ferrar and Karoo magma types, and are similar to those seen in the KwaZulu-Natal region of southern Africa and the Theron Mountains of Antarctica. Olivine-phyric intrusions equilibrated at < 0.5 GPa, and have isotopic compositions (εNd_{182} 1.6-3.6 and $^{87}Sr/^{86}Sr_{182}$ 0.7036-0.7058) that require limited interaction with old continental lithosphere. A suite of plagioclase-phyric intrusions with $^{87}Sr/^{86}Sr_{182}$ c. 0.7035 and εNd_{182} c. +4, and low Th/Ta and La/Ta ratios (c. 1 and c. 15 respectively) also largely escaped interaction with the lithosphere. These isotopically depleted intrusions were probably emplaced synchronously with Gondwana fragmentation and the formation of new oceanic lithosphere. Estimates of mantle potential temperature from olivine equilibration temperatures do not provide unequivocal evidence for the presence of a plume thermal anomaly beneath the Falkland Islands at 182 Ma.

The Early Jurassic (c. 180 Ma) Karoo and Ferrar large igneous provinces (LIP) were associated with Gondwana break-up. Igneous rocks of the Karoo province occur predominantly in South Africa but extend into Dronning Maud Land (Antarctica) with the main phase of activity taking place in the interval 182-183 Ma (Svensen *et al.* 2012). The Ferrar Province, which is contemporaneous with the magmatism in the Karoo province (Burgess *et al.* 2015), is typified by the low TiO_2 Jurassic igneous rocks of the Transantarctic Mountains and Tasmania (Hergt *et al.* 1989; Fleming *et al.* 1995). It has also been established that the Karoo and Ferrar provinces have areas of geographical overlap, most notably in the KwaZulu area of South Africa (Sweeney *et al.* 1994; Riley *et al.* 2006) and in the Theron Mountains of Antarctica (Brewer *et al.* 1992). In the latter, at least four suites of low TiO_2 igneous rocks have been recognized, and it has been suggested that there is a transition from one province to the other rather, than a strict geographical delineation between the two provinces (Brewer *et al.* 1992).

Elliott & Fleming (2000) argued that the principal focus of magmatism for both the Karoo and Ferrar provinces was the Weddell Triple Junction (Fig. 1) which was within the envelope of a plume-related thermal anomaly associated with Gondwana break-up. The near perfect matching of the stratigraphy, structural geology and outcrop pattern of the of the Falkland Islands with that of the eastern Karoo basin, led Adie (1952) to propose a pre-Jurassic plate reconstruction which placed the islands adjacent to the Transkei area of South Africa (Fig. 1a), forming the south-east corner of the Karoo basin with its adjoining Palaeozoic fold belts. Evidence from palaoemagnetic studies (e.g. Mitchell *et al.* 1986; Taylor & Shaw 1989) similarly place the Falkland Islands on the extension of the Cape Fold Belt of South Africa, on the eastern flank of the Lebombo Rift (Fig. 1; Macdonald *et al.* 2003; Stone *et al.* 2008; 2009; Richards *et al.* 2013). Post-180 Ma, there was major re-organization of crustal blocks in Patagonia, the Falklands Plateau and west Antarctica, which included the clockwise rotation of the Falklands crustal block in an overall extensional regime, the early stages of this process being dominated by strike-slip motion between the Antarctic and African plates (Taylor & Shaw 1989). The 180°

rotation of the Falkland Islands from their pre-180 Ma position was complete by 165 Ma (Macdonald *et al.* 2003), and by this time the islands had migrated to the west along the extension of the Aghulas Fracture zone to a position well to the west of the WTJ (Richards *et al.* 2013).

Consequently, the Falkland Islands may have been very close to the focus of break-up related magmatism, and it is logical to assume that the geochemical composition of any igneous rocks found in the islands should reflect the diversity of magmatism in the Jurassic Gondwana LIP as a whole. In this paper, new data are presented that show that the dykes and minor intrusions of the Falkland Islands exhibit variability in mineralogy, major element, trace element and Sr-, Nd- and Pb-isotopic compositions that is nearly as large as that seen in the entire Jurassic Gondwana LIP, even though the Falkland Islands themselves represent only an extremely small area compared to the total distribution of Jurassic igneous rocks of the region. Intrusions with major and trace element characteristics most similar the Ferrar dolerites of the Transantarctic Mountain are juxtaposed with intrusions which are nearly identical to some Karoo basalts of South Africa and Antarctica.

Falkland Islands Dyke Swarm

Dolerite dykes, mostly of Jurassic age, are widespread in West Falkland and rather sparse in East Falkland (Fig. 2; Greenway 1972; Mussett & Taylor 1994; Thistlewood *et al.* 1997; Mitchell *et al.* 1999; Stone *et al.* 2008, 2009; Richards *et al.* 2013). Distinct sub-swarms of dykes have been recognized based on azimuth of exposed intrusions and aeromagnetic anomalies (Mitchell *et al.* 1999; Stone *et al.* 2009). Prominent dolerite dykes, tens of metres wide and oriented NE-SW, are present in both West and East Falkland and are reversely magnetized. This suite corresponds to the N-S suite of Mitchell *et al.* (1999), and is of Jurassic age (c. 178-190 Ma; Mussett & Taylor 1994; Stone *et al.* 2009) although the older of these ages were generated by the Ar-Ar method on whole-rock samples and have large errors (e.g R1790 190±4 Ma; Mussett & Taylor 1994). E-W oriented olivine-dolerite dykes occur locally in the

77 south of West Falkland, and they form part of a larger suite of intrusions that Stone *et al.* (2009)
78 suggest has a partially radial disposition. In addition, Richards *et al.* (2013) noted that there is a
79 suite of about 40, N-S oriented magnetic anomalies, that may represent intrusions, and these
80 occur across the entire Falkland Islands. Exposed examples from Teal Creek and Peat Banks
81 (Fig. 2) yield $^{40}Ar/^{39}Ar$ ages in the range 133-138 Ma and these dykes are likely to be members
82 of the Etendeka suite of south-western Africa (Stone *et al.* 2009; Richards *et al.* 2013). During
83 the current study, $^{40}Ar/^{39}Ar$ step-heating analysis was carried-out on separated plagioclase
84 feldspar phenocrysts from three samples, but only one of these yielded useful information.
85 Sample WI-5, a NE-SW oriented dyke from Weddell Island (Fig. 2), which is also within the
86 area of the radial swarm identified by Richards *et al.* (2013), contains abundant plagioclase
87 phenocrysts, and yielded a precise age of 182.3±1.5 Ma (Fig. 3). This confirms a Jurassic age
88 for some of the Falkland Islands intrusions, and it is within error of the 178.6±4.9 Ma
89 determined by Stone *et al.* (2008) for an aphyric NE-SW dyke from Port Sussex Creek, East
90 Falkland (Fig. 2).

91 Selected major and trace element abundances *versus* weight % MgO for 139 intrusions from
92 the Falkland Islands, including 109 from this study and 30 from Mitchell *et al.* (1999), are
93 shown in Fig. 4 and representative analyses are given in Table 1. Mitchell *et al.* (1999) divided
94 the intrusions of the Falkland Islands into two main N-S and E-W suites based on azimuth, field
95 occurrence, petrography, mineral chemistry and whole-rock geochemical data. A subsidiary
96 three magma types were also tentatively identified by Mitchell *et al.* (1999), including 'evolved
97 N-S', Lively Island and Mount Alice types. The reassessment of the spatial distribution,
98 orientation and age of the dyke swarms by Stone *et al.* (2009) and Richards *et al.* (2013), along
99 with the much enlarged data set for the igneous rocks of the Falkland Islands generated for this
100 study, now allows the identification of five individual geochemical types of intrusions. The
101 criteria used to separate the different groups of intrusions are given in Table 2 and are illustrated
102 in Figs 4 to 9. A description of each suite is given below.

Port Sussex Creek-type intrusions (PST). All the N-S dykes of Mitchell *et al.* (1999) are included in this suite of intrusions, with the exception of the 'evolved type' described by Mitchell *et al.* (1999) which will be discussed under the Dyke Island Type (samples NHF17 and NGF15). PST intrusions are widely distributed across both East Falkland and West Falkland, all are sub-vertical with an azimuth of NE-SW, and they are consistently between 8 and 10 m in thickness. A typical example occurs at Port Sussex Creek, East Falkland, (MHF1; Table 1, Fig. 2), and is an 8m wide, sub-vertical, medium-grained, spheroidally-weathering dolerite dyke with an azimuth of 45º (NE-SW) and an age of 178.6±4.9 Ma (Stone *et al.* 2008). The texture is equigranular and intersertal. Pyroxene is enstatite ($En_{70}Wo_4Fs_{26}$), pigeonite ($En_{51}Wo_{13}Fs_{36}$) and augite (Fig. 5) and the feldspar is labradorite (An_{70}). All PST intrusions contain both augite and pigeonite, with more mafic samples containing orthopyroxene. Olivine (Fo_{50-71}) is rare in this suite of rocks and is restricted to intrusions with Mg# >58 (e.g. FAR1503 and NGF16; Table 1, Fig. 4). Whole-rock MgO contents vary from 5.9-9.5 wt% (Mg# 50-62) and SiO_2 (53-55wt%) is higher for a given MgO concentration than any of the other Falkland Islands intrusions (Fig. 4). The PST intrusions are characterized by low CaO (8.1-9.8wt%) for a given MgO content compared to other Falkland Islands intrusions. TiO_2 abundances (0.9-1.2wt%) are typical of the low TiO_2 Gondwana break-up related LIPs of the southern hemisphere and distinguishes them from the high TiO_2 (>2.5wt%) suite of break-up related magmas (e.g. Brewer *et al.* 1992). Abundances of Cr are unusually high (up to 648ppm) for samples with SiO_2 in their range, and are reflected in the high Cr content of orthopyroxene. Abundances of Nb and Y are restricted to 2-5 and 19-23ppm respectively. PST intrusions are LREE enriched (Fig. 6) with $[La/Yb]_N$ in the range 3.2-3.9 and samples lack any significant Eu anomaly (Eu/Eu* 0.89-0.97). La/Ta and Th/Ta are the highest of any of the Falkland Islands samples analysed (44-52 and 5.9-8.6 respectively), and consequently, on ORB-normalized multi-element diagrams (Fig. 7), samples exhibit a marked trough in the abundances of Ta and Nb relative to Th, U, K and La. $[Ta/Yb]_N$ is in the range 2.0 to 2.6, the lowest values for any of the Falkland Islands intrusions. Ti/Zr and

P/Zr (55-60 and 4.5-6.3 respectively) are such that all PST intrusions exhibit a minor trough at Ti and P relative to adjacent elements on ORB-normalized diagrams. εNd_{182} varies from -5.5 to -11.0 and is accompanied by radiogenic Sr-isotopic compositions ($^{87}Sr/^{86}Sr_{182}$ 0.7070-0.7134), although Sr-Nd isotope covariations are rather scattered (Fig. 8). Pb-isotopic compositions form an array that is close to the Geochron ($^{207}Pb/^{204}Pb$ =15.55-15.65), and extends to $^{206}Pb/^{204}Pb$ ratios of up to 18.40. $^{207}Pb/^{204}Pb$ exhibits a negative correlation with εNd_{182} for PST intrusions (Fig. 8). Marked negative correlations between 1/Sr and $^{87}Sr/^{86}Sr_{182}$, εNd_{182} and Th/Ta and a positive correlation between MgO and εNd_{182} (Fig. 9) suggests that PST dykes underwent interaction with a high $^{87}Sr/^{86}Sr_{182}$ (> 0.714), low εNd_{182} (< -12) component that had Th/Ta > 9, and that interaction was concomitant with crystallization

E-W intrusions. The E-W samples reported by Mitchell *et al*. (1999) are from a single intrusion, approximately 10m wide, which can be traced for more than 30 km from Fox Bay West to Queen Charlotte Bay (Fig. 2). These samples are generally medium-grained olivine-phyric dolerites (Fo_{82} at 11wt% MgO in the whole-rock), the only pyroxene present being augite (Fig. 5). During the current study, intrusions with similar petrographic and mineralogical characteristics were found around South Harbour and on Weddell Island (Fig. 2). E-W intrusions are distinguished from the PST (Fig. 10) by their lower SiO_2 contents (48-52wt%) and higher Ti/Zr (80-95) for a similar range in TiO_2, and MgO content (1.0-1.4 and 4.8-11.4wt % respectively). E-W intrusions have $[La/Yb]_N$ in the range 2.1-4.0 (Fig. 6) and no appreciable Eu anomaly (Eu/Eu* 0.89-1.0). $[Ta/Yb]_N$ ratios are in the range 2.8 to 4.7, and all samples exhibit a negative Nb, Ta trough relative to the LILE (La/Ta, 16-27, Th/Ta 2.2-2.8) but this is not as pronounced as that for the PST intrusions (Fig. 7). E-W intrusions have isotopic compositions that are close to, or slightly depleted relative to the Chondritic Uniform Reservoir (εNd_{182} = -0.4 to 3.0; $^{87}Sr/^{86}Sr_{182}$= 0.7036-0.7058) and have Pb-isotopic compositions that lie just above the NHRL (Fig. 8).

154 ***Lively Island intrusion.*** A single 30m thick intrusion which is exposed on Lively Island has
155 noticeably lower TiO_2 for a given MgO content than any other of the Falklands Islands
156 intrusions (TiO_2 = 0.8wt% at 6wt% MgO) and the data falls close to the compositional trend for
157 low TiO_2 Ferrar dolerites from the Transantarctic Mountains (Fig. 11). Characteristic
158 mineralogical features are the presence of sparse, Mg-rich biotite and rare Ca-poor groundmass
159 pyroxene (Fig. 5). The intrusion has a LREE-enriched REE profile ($[La/Yb]_N$ = 3.2; Fig. 6)
160 which lacks a significant negative Eu anomaly (Eu/Eu* = 0.87). La/Ta and Th/Ta (20.4 and 3.2
161 respectively) are similar to E-W intrusions and considerably lower than for PST intrusions
162 (Table 2). The Lively Island intrusion contains radiogenic Nd and unradiogenic Sr (εNd_{182} -0.5,
163 $^{87}Sr/^{86}Sr_{182}$ c. 0.7060) compared to PST intrusions.
164 ***Dyke Island Type (DIT).*** The greatest concentration of DIT intrusions is on aptly-named Dyke
165 Island (Fig. 2). Sample WI-5 which yielded the Ar-Ar age of 182.3±1.5 Ma which crops out on
166 Weddell Island (Fig. 2) is of this type. In addition, the evolved N-S samples described by
167 Mitchell *et al.* (1999) are of this type (e.g. NHF17; Fig. 2). Intrusions are generally <50 cm
168 thick, they may contain abundant plagioclase ± augite phenocrysts (samples WI-5, MHF14.9
169 and FAR338; Fig. 5), or more commonly they are medium- to fined-grained aphyric basaltic-
170 andesites and andesites with rare rhyolite sheets occurring locally. DIT intrusions represent an
171 expanded fractionation series with MgO varying from 5.6 to <0.1wt%, over a range of 51-
172 75wt% SiO_2. Ti/Zr is in the range 32-55 for samples with 4.0-5.6wt% MgO, and for samples
173 with <1wt% MgO, Ti/Zr falls to <5 (Fig. 4). All DIT intrusions have higher concentrations of
174 the incompatible elements Zr, Nb and Y than any of the other intrusions from the Falkland
175 Islands, and exhibit strong positive linear correlations between these elements. On a plot of TiO_2
176 *versus* MgO (Figs 4 & 11) DIT intrusions can be divided into three distinct series; i) a low TiO_2
177 series which forms and extension of the data array for PST intrusions; ii) a high TiO_2 series with
178 MgO in the range 2.5-4.0wt% MgO with TiO_2 >1.7wt%; and iii) acid intrusions with <2wt%
179 MgO.

DIT intrusions are LREE-enriched ($[La/Yb]_N$ = 4.1-6.6; Fig. 6) and exhibit stepwise increases in both LREE and HREE abundances with decreasing MgO with the most evolved sample (MHF41.3, 0.06wt% MgO) having La_N = 190 and Yb_N = 44. The development of a progressively larger negative Eu anomaly (Eu/Eu* 0.85-0.71) with decreasing MgO, attests to the importance of plagioclase fractionation during their petrogenesis. Th/Ta and La/Ta for the DIT intrusions (2.4-3.4 and 17-26 respectively) are similar to those for the E-W intrusions. Multi-element diagrams (Fig. 7) show that DIT intrusions exhibit troughs at Ti and P relative to adjacent elements, and a progressively larger negative Sr anomaly is developed with decreasing MgO. Plagioclase-phyric samples WI-5 and FAR338 exhibit a positive Sr spike in Fig. 7, which is presumably a result of accumulation of plagioclase feldspar, although neither sample exhibits a Eu anomaly. The distribution of trace elements in DIT intrusions bears a strong resemblance to those for Ferrar dolerites from the Transantarctic Mountains (Fig. 7). DIT intrusions have $^{87}Sr/^{86}Sr_{182}$ in the range 0.7055-0.7170 but all samples with $^{87}Sr/^{86}Sr_{182} > 0.7090$ contain < 2 weight % MgO. εNd_{182} falls in the range -2.8 to +0.6, and there is no systematic variation between MgO, εNd_{182} or $^{87}Sr/^{86}Sr_{182}$ (Figs 8 & 9).

Mount Alice Type intrusions (MAT). MAT intrusions are restricted to the south-western area of West Falkland, around South Harbour, Dyke Island and Cape Orford (Fig.1) and are early Jurassic in age (188±2 Ma for sample MA3; Mussett & Taylor 1994). MAT intrusions are generally <1 m thick and are characterized by plagioclase ± augite ± olivine phenocrysts in a fine-grained groundmass. Since the area in which the MAT intrusions occur is within the region of the radial dyke swarm described Richards *et al.* (2013), azimuths cannot be used as one of their classification criteria, although in the region of Cape Orford, MAT dykes are generally oriented E-W (Mussett & Taylor 1994; Thistlewood *et al.* 1997). A typical example (MFH15.2) contains sparse, scattered phenocrysts of olivine (Fo_{80}), calcic augite ($En_{31}Fs_{25}Wo_{44}$; Fig. 5) and labradorite (An_{60}). MgO varies from 6-12wt%, and the MAT intrusions have the lowest SiO_2 (46-50wt%) for a given MgO content of any of the Falklands Islands samples (Fig. 4). TiO_2

206 abundances (1.3-2.0wt%) overlap with those for both the PST and E-W intrusions but Ti/Zr is in
207 the range 90-150 (Fig. 10) which is considerably higher than any other of the Falkland Islands
208 intrusions. MAT intrusions have $[La/Yb]_N$ in the range 1.8-3.1 (Fig. 6) and flat to slightly
209 LREE-depleted REE profiles for elements La to Sm ($[La/Sm]_N$ 0.9-1.5). On multi-element
210 diagrams (Fig. 7), MAT intrusions exhibit a positive Sr spike relative to N-ORB, but otherwise
211 have smooth profiles from elements Nd to Lu, with Ti/Zr and P/Zr (98-130 and 8.0-10.4
212 respectively) in the range for normal ORB (Ti/Zr c. 100, P/Zr c. 6.9; Sun & McDonough 1987).
213 Unlike all the other Falkland Islands intrusions, the MAT have Th/Ta and La/Ta (0.7-1.0 and
214 13-17 respectively) which are also within the range for normal ocean ridge basalts and
215 asthenosphere-derived basalts (Sun & McDonough 1987). Sr- & Nd-isotopic compositions fall
216 in the upper-left quadrant of Fig. 8, with $\varepsilon Nd_{182}>5$ and $^{87}Sr/^{86}Sr_{182}<0.7040$. Pb-isotopic
217 compositions fall just above the NHRL with $^{206}Pb/^{204}Pb$ in the range 18.2-18.5 (Fig. 8).

218 ## Petrogenesis of the Falkland Islands intrusions

219 The diversity of major and trace element geochemistry and isotopic compositions of the
220 Falkland Islands intrusions requires an equally diverse range of petrogenetic histories. In
221 particular, the observed ranges of isotopic compositions described above are likely to require
222 variable interaction between isotopically depleted melts from mantle peridotite with melts
223 derived from continental lithosphere, which in some cases, must of considerable antiquity.
224 Consequently, before attempting to make regional comparisons between the Falkland Islands
225 intrusions and other Gondwana break-up related low TiO_2 suites within the southern
226 hemisphere, an assessment of the petrogenetic history of each of the suites of Falkland Island
227 intrusions will be made in turn below.

228 ***PST intrusions***

229 PST and low TiO_2 DIT intrusions exhibit variations in major element compositions that fall
230 along the same fractionation trend as low TiO_2 basaltic-andesites and andesites from the Theron

231 Mountains (Fig. 11). However, PST and DIT intrusions cannot be related to one another by
232 simple crystal fractionation because their Sr-, Nd- and Pb-isotopic compositions differ
233 significantly from one another (Fig. 8). The high $^{87}Sr/^{86}Sr_{182}$ (>0.710) and unradiogenic Nd-
234 isotopic compositions of the PST is a feature they share with Ferrar Province igneous rocks.
235 Fleming *et al.* (1995) and Molzhan *et al.* (1999) demonstrated that elevated $^{87}Sr/^{86}Sr_{182}$ (0.7090-
236 0.7112) of MFCT basalts was partly a function of Rb and Sr mobility during a Cretaceous (97-
237 125 Ma) hydrothermal event. However, the observed range in εNd_{182} in the same samples (-4.8
238 to -5.6) is unlikely to be the result of alteration, and Fleming *et al.* (1995) concluded from
239 analysis of phenocryst pahses, that prior to alteration, MFCT basalts must have had
240 $^{87}Sr/^{86}Sr_{182} \geq 0.7090$. Alteration by the same regional hydrothermal thermal event cannot be used
241 as an explanation for variability in the Sr-isotopic compositions of PST intrusions because the
242 Falkland Islands would have already broken-away from the Antarctic continent by this time. In
243 addition, the range of εNd_{182} from -6 to -12 over the limited range of $^{87}Sr/^{86}Sr_{182}$ = 0.7110-
244 0.7115, for the PST intrusions, requires potential contaminants that had a range of Nd-isotopic
245 compositions and were therefore probably of differing ages.
246 **Interaction with the continental lithosphere.** For the PST intrusions, the variations shown in
247 Fig. 9 indicate that Sr- and Nd-isotopic variations were imposed on the magmas concomitant
248 with fractional crystallization, by assimilation with fractional crystallization (AFC) or a similar
249 process. The relationships shown in Fig. 9 require that Sr behaved incompatibly during
250 fractional crystallization of the PST suite. The crystal cumulate formed during AFC cannot,
251 therefore, have been plagioclase-rich. To generate the range of Sr-isotopic compositions seen in
252 the PST intrusions requires a source with $^{87}Sr/^{86}Sr_{182} \leq 0.7075$, and contaminants with
253 $^{87}Sr/^{86}Sr_{182} > 0.7130$ and a range of εNd_{182}, which must be ≤ -6.0 for all samples. Least-squares
254 modelling of the extract and evolved liquid from a starting composition with 9.6wt% MgO
255 (NGF16) to evolved composition with 6.78wt% MgO (MHF5.1; Table 3) requires 21%
256 crystallization of an assemblage of orthopyroxene (74.7%), plagioclase (18.9%) and minor

augite (6.4%). With only 18.9% of the fractionating assemblage being plagioclase, D_{Sr} would have been <1 which is consistent with the relationship between 1/Sr and $^{87}Sr/^{86}Sr_{182}$ in Fig. 9. In addition, Demarchi *et al.* (2001) showed that orthopyroxene is on the liquidus of Ferrar tholeiites at 1.0-1.5 GPa, suggesting that magmatic differentiation of the PST intrusions occurred a depths ≥30 km.

Sr- and Nd-isotopic compositions for PST intrusions fall in an intermediate position between the data for CT1 basalts of Dronning Maud Land and the Karoo (Fig. 12). Luttinen & Furnes (2000) argued that the extreme Nd-isotopic compositions ($\varepsilon Nd_{182} \leq -17$) of CT1 basalts were the result of interaction between a mantle-derived magma and Archean (3.0 Ga) Grunehogna cratonic lithosphere (Fig. 1). Riley *et al.* (2006) used AFC and energy-constrained recharge AFC to model the isotopic compositions of Karoo basaltic rocks using an ORB-like source and an assimilant with $\varepsilon Nd_{182} = -4$ and $^{87}Sr/^{86}Sr_{182} = 0.710$, and showed that the observed isotopic variability in the basalts could be explained partly by these processes. In Fig. 12 three AFC trajectories are plotted and the parameters used to generate the curves are given in Table 4. These are not designed to fully explain the isotopic diversity in Gondwana low TiO_2 continental flood basalts, they have been generated in an attempt to constrain possible and impossible petrogenetic processes. The starting composition has been kept constant, and is based on that of largely uncontaminated low TiO_2 basalts with $\varepsilon Nd_{182} = 2$ and $^{87}Sr/^{86}Sr_{182} = 0.7035$. For all three modelled AFC trends, the ratio of the country rock assimilated to crystal cumulate formed, R, has be set at 0.40, a value that is appropriate for crystallization in the middle- to upper-crust (Riley *et al.* 2006; Hole *et al*. 2015). D_{Sr} and D_{Nd} are set at 0.5 and 0.1 respectively, to simulate a cumulate with approximately 25% plagioclase, and 75% ferromagnesian minerals. This means that all three AFC trajectories approach the composition of the most contaminated magma for ≤ 20% AFC (Table 4). Increasing the value of R to 0.5 for any of the models does not significantly change the shape of the trajectories, but decreases the amount of AFC that is needed to reach the target compositions to ≤12%., and conversely, decreasing R to 0.3 requires ≤ 25% AFC. For the

283 CT1 AFC model, the contaminant represents 3.0 Ga Grunehogna Craton (Fig. 1) felsic granulite,
284 with εNd_{182} = -50 and $^{87}Sr/^{86}Sr_{182}$ = 0.712 (felsic xenolith sample X4-AVL of Luttinen & Furnes
285 2000). The PST-1, mixing line intersects the lowest εNd_{182} samples in the PST suite, and the
286 contaminant represents a 2.2 Ga Palaeoproterzoic felsic granulite with εNd_{182} = -20 and
287 $^{87}Sr/^{86}Sr_{182}$ = 0.720 (Luttinen & Furnes 2000). The PST-2 mixing line, which also intersects the
288 majority of data for Karoo basalts and lowest $^{87}Sr/^{86}Sr_{182}$ (~0.7090) samples of Ferrar igneous
289 rocks, representing mixing between a mantle-derived magma and 1.0-1.5 Ga felsic crust with
290 εNd_{182} = -10 and is the same contaminant as that suggested by Riley *et al.* (2006) for Karoo
291 basalts. Plate reconstructions place the Falkland Islands mainly within the 1.0-1.5 Ga
292 Namaqualand-Natal-Maudheim-Mozambique belt (Thistlewood *et al.* 1997) and on the
293 continuation of the Cape Fold Belt (Fig. 1). Mesoproterozoic crust is therefore a likely candidate
294 for basement to the Falkland Islands, although there are no isotopic data for the Cape Meredith
295 metamorphic complex. What is also clear is that cratonic basement like that involved in the
296 petrogensis of the CT1 basalts affected neither the PST intrusions nor Karoo low TiO_2 basaltic
297 rocks. AFC models with geologically reasonable parameters and appropriate ages of potential
298 basement contaminants can therefore produce the observed variations in the Sr- and Nd-isotopic
299 characteristics of the PST intrusions for <20% AFC.

300 **Pyroxenite *versus* peridotite sources.** PST intrusions with MgO > 8 weight % have lower CaO
301 abundances (c. 8.5 weight %) than any other of the other Falkland Islands intrusions (Figs. 4 and
302 13). Such compositions are uncommon in continental flood basalts provinces. Orthopyroxene
303 was the dominant fractionating phase during crystallization of the PST (Table 3) and estimates
304 of more primitive compositions can be calculated by incrementally adding enstatite to a mafic
305 PST composition. Addition of 30% enstatite to sample NGF16 yields magma with ~15wt%
306 MgO and ~7.5wt% CaO. Compositions such as these are also found in the CT1 basalts of
307 Dronning Maud Land (Fig. 13a). An unusual feature of the PST intrusions is their Si-

oversaturated nature and high Cr content (Fig. 13b) which is also reflected in unusually high Cr content of component orthopyroxene (e.g. enstatite in MHF3.2 has 0.74wt% Cr_2O_3 at MgO/FeO = 2.8). In terms of major element compositions, PST intrusions bear strong similarities with magnesian andesite from continental subduction settings (e.g. Baker *et al.* 1994; Sato *et al.* 2014). For example, high-Mg andesites from Mt Shasta have a similar range of MgO to PST intrusions (Fig. 13a) which is accompanied by SiO_2 = 51.5-54.0wt%, Cr = 245-695 ppm, Ni =99-235 ppm, TiO_2 = 0.6-0.8wt% and CaO =8.6-9.6wt%. One mechanism that has been suggested for the production of high-Mg andesite is the interaction of slab-derived adakitic melts with mantle peridotite during subduction (Heinonen *et al.* 2014). A link to the previous subduction history of the mantle source from which Ferrar and Karoo basaltic rocks were derived has been made by a number of workers (e.g. Brewer *et al.* 1992; Storey *et al.* 1992; Heinonen *et al.* 2014) and in particular, the characteristic trough at Nb and Ta relative to adjacent elements (Fig. 7) has been interpreted as an inherited subduction signature.

Herzberg & Asimow (2008) note that primary magmas derived from the melting of pyroxenite will exhibit relative CaO depletion compared to melts from a peridotite source because of the dominance of residual clinopyroxene in the source region during partial melting of pyroxenite. Given the position that data for the PST occupy in Fig. 12, it seems clear that their major element compositions are not consistent with an origin by melting of mantle peridotite. It is well established that pyroxenite can be formed at the base of the lithosphere as a result of accumulation of mafic phases during basaltic magmatism (e.g. Downes *et al.* 2007). Such accumulative pyroxenite can yield magma by partial melting at some later stage, promoted by a new phase of mafic magmatism and by interaction with peridotite-derived melts (Lambart *et al.* 2013). The generation of silica-enriched pyroxenite melts is possible, which can yield Si-oversaturated melts like those of the PST intrusions (Lambart *et al.* 2013). It is therefore suggested that the PST were derived from a pyroxenite-rich source that was emplaced at the base of the lithosphere during the prolonged subduction history of Gondwana. Metasomatism of

334 the pyroxenite by slab-derived fluids and melt, imparted a subduction signature to the
335 pyroxenite. When subjected to the high mantle potential temperatures associated with the mantle
336 plume beneath Dronning Maud Land at c. 180 Ma (T_P up to 1600°C; Heinonen *et al.* 2010), the
337 pyroxenite underwent partial melting and produced the primary melt precursor to the PST
338 intrusions. These melts then interacted with fusible, felsic continental crust to produce the
339 geochemical composition of the more evolved PST compositions by AFC, or a related process.
340 Extrapolation of the MgO - εNd_{182} trend for the PST to higher MgO contents (Fig. 9a), suggests
341 that a primitive composition with 15 weight % MgO might have had εNd_{182} ~0, and the
342 correlation between 1/Sr and Sr-isotopic compositions requires the source to have $^{87}Sr/^{86}Sr_{182} \leq$
343 0.7075.

344 ***E-W intrusions***

345 Least-squares modelling of the extract and evolved liquid from a starting composition ECF12 to
346 more evolved sample ECF44 (Table 3) requires crystal fractionation of 57% olivine and 40%
347 plagioclase feldspar with little contribution from augite (c. 2.6 %) which is a typical
348 crystallizing assemblage for tholeiitic melts at pressures ≤0.5 GPa (e.g. Hole & Morrison 1992;
349 Villiger *et al*. (2007), requiring E-W intrusions to have last equilibrated at <~15 km depth,
350 within the crust. This is in contrast to the >1.0 GPa equilibration required by PST intrusions.
351 The isotopic compositions of E-W intrusions require derivation from a depleted mantle source
352 (Figs 8), but they have higher Th/Ta (2.2-2.8) and La/Ta (16.4-26.1) than would be expected if
353 they were derived from asthenospheric mantle (Th/Ta~1.0 and La/Ta≤18; Sun & Mcdonough
354 1989) and they also exhibit a noticeable trough at Nb and Ta relative to adjacent elements in
355 Fig. 7, a feature that is most often attributed to interaction with continental lithosphere.
356 However, the extent of this interaction must either have been limited, or the source from which
357 the E-W intrusions were derived had a Th/Ta>2.0 and La/Ta>26. The low pressure
358 equilibration of E-W intrusions, coupled with their depleted isotopic compositions may suggest

359 thet they were emplaced during a period of crustal attenuation and were thus able to escape
360 interaction with continental lithosphere.

361 ***DIT and Lively Island intrusions***

362 In contrast to the PST intrusions, the sub-horizontal arrays delineated by DIT intrusions in Fig.
363 9a, suggests that AFC or a similar process was not important during their petrogenesis.
364 However, a negative correlation between Th/Ta and εNd_{182} for the DIT intrusions (Fig. 9b) may
365 require minor modification by a crustal component with Th/Ta≥3.0. A characteristic feature of
366 the DIT samples is that they have εNd_{182} in range -2.8 to +0.6, but with only a single analysed
367 sample (NHF17) having εNd_{182}<-1. In addition, the Lively Island dyke, which falls close to the
368 fractionation trend for the MFCT basaltic rocks of the Transantarctic Mountains (Fig. 11), has
369 Sr- and Nd-isotopic compositions ($^{87}Sr/^{86}Sr_{182}$ c. 0.7052, εNd_{182} = -0.5 to -1.4) that do not
370 require the significant isotopic enrichment seen in the Ferrar dolerites (εNd_{182} in the range -3.3
371 to -5.3; Fleming *et al.* 1995; Hergt *et al.* 1989). The source of the low TiO_2 DIT magmas could,
372 therefore, have had εNd_{182}>0, $^{87}Sr/^{86}Sr_{182}$<0.7050, Th/Ta<2.5 and La/Ta<20.

373 ***MAT intrusions***

374 The positive εNd_{182} (2.7-3.6) and low Th/Ta, La/Ta and $[La/Yb]_N$ (0.8-1.0; 12.8-17.3 and 1.9-
375 3.7 respectively) of MAT intrusions suggests that they were derived from an asthenospheric
376 source, and escaped significant interaction with lithosphere. The most satisfactory explanation
377 for the geochemical compositions of these rocks is that they were generated by decompression
378 melting of the asthenosphere during the rifting stage of Gondwana break-up. In this respect they
379 have similar geochemical compositions to the ORB-like Rooi Rand basaltic dykes of the
380 southern Lebombo (Cox & Bristow 1984, which post-date the main magmatic phases in the
381 region by about 5 Myr (Jourdan *et al.* 2007).

382 ***Cretaceous intrusions***

Until more data are forthcoming, the origin and affinity of the Cretaceous Teal Creek intrusion reported by Stone *et al.* (2009) remains somewhat obscure. Major element data for the intrusion plot close to the Theron Mountains low TiO_2 trend in Fig. 6, but the intrusion has higher Fe_2O_3 (c. 15.9wt%) at 5.7wt% MgO than any of the data for the intrusions presented here. What is clear, is that there is an extensive suite of low TiO_2 basalts within the Etendeka Province (e.g. Gibson *et al.* 2005; Thompson *et al.* 2001) from which it could be related. However, none of the groups of intrusions described here carries a similar signature to that presented by Stone *et al.* (2009) for the Teal Creak dyke.

Provinciality and chemical affinities of Falkland Islands intrusions

A number of authors have noted that there are spatially constrained variations in major and trace element compositions within the Jurassic Gondwana break-up related flood basalts provinces of the Southern Hemisphere (e.g. Brewer *et al.* 1992; Luttinen & Furnes 2000; Riley *et al.* 2006). Figs 11 and 14 illustrate the variability in abundances of MgO, TiO_2, SiO_2 and Ti/Zr for Falkland Island intrusions, along with igneous rocks which are defined as being either Karoo or Ferrar magma types, or those which are considered to be transitional between the two magma types (Brewer *et al*. 1992; Luttinen & Furnes 2000; Riley *et al.* 2006). In the following sections, we will examine the geochemical affinities of the Falklands Islands intrusions in relationship to other early Jurassic flood basalts of Gondwana.

PST intrusions

PST intrusions exhibit strong similarities to CT1 basalts of Dronning Maud Land (e.g. Fig. 14), and show some overlap with the compositional field for samples from the Theron Mountains and Transantarctic Mountains. In terms of incompatible trace elements, PST dykes exhibit almost identical multi-elements patterns to sample SA.6.1 (Fig. 7; Riley *et al.* 2006) from KwaZulu-Natal, with which they share also unradiogenic Nd-isotopic compositions (e.g. SA.6.1 εNd_{182} = -8.9). Within the CT1 basalts of Dronning Maud Land, very similar compositions to PST intrusions can be found (e.g. B70-AVL; Luttinen & Furnes 2000) again with many basalts

409 in the CT1 suite having unradiogenic Nd-isotopic compositions (Fig. 12). Furthermore, both
410 CT1 and PST magmas required derivation from a pyroxenite-rich, CaO deficient, source region
411 (Fig. 13). It is with some confidence that we conclude that the PST, CT1 and some KwaZulu-
412 Natal basalts were derived from very similar source regions, had similar petrogenetic histories
413 and represent the same phase of pre-break-up magmatism.

414 ***E-W intrusions***

415 These igneous rocks exhibit a strong geochemical affinity with basalts from Kirwanveggan
416 (Harris *et al.* 1990) and Schirmaker Oasis (Sushchevskaya *et al.* 2009), Dronning Maud Land
417 (Figs 11 and 14). A notable characteristic of all the above samples is that they have radiogenic
418 Nd-isotopic compositions (εNd_{182} = 2-6) $^{87}Sr/^{86}Sr_{182}$ in the restricted range 0.7040-0.7060 and
419 $^{206}Pb/^{204}Pb$ in the range 17.97-18.49 and plot close to the NHRL in Fig. 8. These isotopic
420 characteristics, coupled with Ti/Zr = 70-90 and SiO_2 = 47.0-52.8wt%, clearly separates
421 Kirwanveggan, Schirmaker Oasis and Falkand Islands E-W intrusions from PST intrusions. E-
422 W intrusions also fall within the compositional field for basalts from the Central Karoo of South
423 Africa in Fig. 14, and intrusions with compositions similar to those of Falkland Islands E-W
424 intrusions are prevalent in the Golden Valley Sill Complex (Neumann *et al.* 2011).

425 ***DIT and Lively Island intrusions***

426 In Fig. 14b, DIT intrusions exhibit almost complete overlap with the MFCT Ferrar dolerites of
427 the Transantarctic Mountains. However, consideration of Fig. 11, shows that DIT intrusions are
428 not of the same low TiO_2 (<0.5-1.2wt%) lineage of the MFCT. However, DIT intrusions do
429 have compositions that overlap with those for low TiO_2 Theron Mountains basalts and samples
430 from KwaZulul-Natal that Riley *et al*. (2006) and Brewer *et al.* (1992) argued were transitional
431 between Ferrar and Karoo magma types. We concur with this hypothesis, and given the position
432 that the Falkland Islands occupied in southern Gondwana at the time of Karoo and Ferrar
433 magmatism, this seems entirely reasonable.

The Lively Island intrusion is the only member of the intrusive suite of rocks of the Falkland Islands that falls within the compositional range for MFCT samples from the Transantarctic Mountains in Figs 11 and 14. However, the Lively Island intrusion has considerably lower La/Ta and Th/Ta (20.5 and 3.2 respectively) than the majority of the MFCT dolerites (La/Ta 19-47; Th/Ta 4.3-23.3), and the Lively Island dyke also has considerably more radiogenic Nd (εNd_{182} = -0.5 to -1.4) than MCFT dolerites (εNd_{182} = -4.7 to -5.7). It is important to note, that the Lively Island intrusion is a single body of igneous rock around 30m thick, and consequently is not a volumetrically significant part of the Falkland Islands dyke swarm.

MAT intrusions

Ti/Zr>90 coupled with SiO_2 of 45.7-51.0wt% are characteristics that MAT intrusions share with CT2 and CT3 basalts from Dronning Maud Land and samples from the Rooi Rand dyke swarm of the southern Lebombo area of southern Africa (Cox & Bristow 1984).. The unradiogenic Sr-isotopic compositions ($^{87}Sr/^{86}Sr_{182}$ c. 0.7040) and radiogenic Nd-isotopic compositions (εNd_{182} = 2.5-4.0) of E-W intrusions also characterize Rooi Rand and CT2 and CT3 basalts, although the Dronning Maud Land samples have a rather more extended range of isotopic compositions, which Luttinen & Furnes (2000) attribute to conservative amounts of interaction with upper-crustal felsic contaminants.

Mantle potential temperature, rifting and magmatism

Fig. 15a summarizes the available data for olivine equilibration temperatures (T_{OL}) for MAT and E-W basalts and picrites from Dronning Maud. MAT and E-W basalts yield olivine equilibration temperatures of 1245°C and 1330°C respectively, using the method of Putirka *et al.* (2007), whilst olivine in picrites from Dronning Maud Land yield T_{OL} up to 1450°C. Converting equilibration temperatures to T_P is problematical if the pressure and extent of melting cannot be independently determined (Herzburg & Asomow 2008; Herzburg & Gazel 2009; Hole 2015), which they cannot for the MAT and E-W samples. However, since olivine equilibration temperature increases with increasing pressure of crystallization, synthetic olivine

460 liquidi can be calculated for any given temperature and pressure (Herzberg & Gazel 2009). Fig.
461 15b shows the inferred temperature-pressure conditions at which fractional melting terminated
462 for calculated primary magmas from Dronning Maud Land, the Karoo Province of southern
463 Africa, Ferrar dolerites of Antarctica. (Hole 2015). In Fig. 15c, data for basalts from the
464 Cretaceous Etendeka Province of SW Africa (Kieding *et al.* 2011) are given, for which
465 estimates of T_{OL}, estimates of T_P from melt inclusions in ultra-magnesian olivine, and estimates
466 of T_P from the PRIMEL2 model of Herzberg & Asimow (2008) have all been calculated on the
467 same samples. Using the Herzberg & Asimow (2008) model yields T_P = 1500-1550°C and final
468 pressures of melting (P*f*) between 1.5 and 4.0 GPa (Fig. 13c). T_P from melt inclusions is 1300-
469 1520°C, whilst T_{OL} is in the range 1250-1400°C and there is an empirical relationship between
470 T_{OL} and melt inclusion T_P which approximates to $T_P = 1.443 \times T_{ol} - 501$ for the Etendeka plume
471 system (Fig. 15). Therefore is seems that within a single plume system, basalts may be
472 generated over ranges of T_P that are larger than the ±50°C error inherent in the calculation
473 methods (Herzberg & Asimow 2009; Hole 2015). Direct application of this empirical
474 observation to the Dronning Maud Land picrites suggest maximum T_P~1550°C, a temperature
475 that is considered to be associated with 'hot' mantle plumes such as Iceland at 60 Ma (Fig. 15;
476 Herzberg & Gazel 2009). For Falkland Islands E-W basalts, T_{OL}~1330°C, which implies
477 T_P~1400°C and for olivine-phyric MAT basalts, T_{OL}~1250°C implying T_P~1300°C. These T_P
478 estimates for the Falkland Islands E-W and MAT basalts may therefore be reconciled with a
479 model involving melting of mantle with near-ambient temperature ($T_P \geq 1350$°C), but would
480 require intersection of the dry peridotite solidus at ~2.1 GPa (~70km) and all melting to take
481 place in the spinel stability field of the mantle; the most mafic MAT and E-W intrusions have
482 $[La/Yb]_N$ <2.0 which does not preclude such an origin. Additionally, near-ambient T_P melting
483 would require the continental lithosphere to be thinned substantially and perhaps to < 50km, to
484 allow decompression melting to take place. The depleted isotopic compositions of the E-W and
485 MAT intrusions, along with the <0.5 GPa equilibration of the E-W magmas, provides additional

evidence to suggest that these intrusions were emplaced during a period of crustal stretching, possible coeval with the initiation of Gondwana. Nevertheless, whilst there is no primary evidence to suggest T_P was >1450°C beneath the Falkland Islands at 180 Ma, it is possible that high-MgO large melt fractions requiring substantially higher T_P exist in the region, but have not been sampled, remains a possibility.

The diversity of magma types found in the Falkland Islands, and the position in Gondwana which the islands occupied during magmatism (Fig. 1) is entirely consistent with the their being close to the focus of magmatism during continental break-up. We concur with Brewer *et al*. (1992) and Riley *et al*. (2006) that there is considerable overlap in the geographical distribution of the Ferrar and Karoo LIPs, which is most obvious in the Theron Mountains and Falkland Islands. It is also clear, that despite the wealth of geochemical data available for the Transantarctic Mountains and Tasmania, there is no evidence to suggest that volcanic rocks with affinities to the Karoo LIP occur in those areas. With the exception of the ORB-like basalts of the Rooi Rand dyke swarm (Marsh *et al.* 1997; Mitchell *et al.* 1999) which are likely to represent syn-break-up magmas, basaltic rocks with Karoo-type geochemical compositions only extend as far south as the overlap zone in the Theron Mountains.

Conclusions

The Jurassic (c. 182 Ma) intrusions of the Falkland Islands exhibit a broad range of geochemical compositions and at least four main petrogenetic lineages are recognized. PST intrusions were derived by melting of an isotopically-enriched pyroxenite-rich source, followed by orthopyroxene-dominated crystal fractionation at ≥1 GPa. Pyroxenite-derived PST magmas subsequently interacted with 'old' (≥2.2 Ga) fusible continental lithospheric components by AFC or a related process. The geochemical compositions of DIT intrusions bear striking similarities to igneous rocks of Kwazulu-Natal and the Theron Mountains, which are considered to be transitional in composition between those of the Ferrar and Karoo magma types. A significant number of mafic (Mg# 50-62) E-W and MAT intrusions possess radiogenic Nd- and

512 unradiogenic Sr-isotopic compositions ($^{87}Sr/^{86}Sr_{182}$<0.7050 and εNd_{182}>2.5), also have Th/Ta
513 and La/Ta (<3.0 and <25 respectively) that require little input from the continental lithosphere.
514 In addition, E-W intrusions carry mineralogical and chemical fingerprints of equilibration at <
515 0.5 GPa. E-W and MAT basalts were probably emplaced during rifting and continental break-up
516 and are likened to the Rooi Rand dykes of the Southern Lebombo of Africa. However, there is
517 currently no evidence to suggest that the Falkland Islands intrusions were derived by melting
518 above a significant mantle thermal anomaly. Early Jurassic plate reconstructions place the
519 Falkland Islands close to the Weddell Triple Junction, perhaps explaining the diversity of
520 igneous rock compositions found in a relatively limited geographical region.

521 **Acknowledgements.**
522 An earlier version of the manuscript was improved by thoughtful comments from two
523 anonymous reviewers. Dr D. Aldis, Falkland Islands Geological Survey, is thanked for
524 providing some samples from Fox Bay West for this study.
525

References Cited.

Adie, R.J. 1952. The position of the Falklands Islands in a construction of Gondwanaland. *Geological Magazine*, **89**, 401-410.

Antonini, P., Piccirillo, E.M., Petrini, R., Civetta, M., D'Antonio, M. & Orsi, G. 1999. Enriched mantle Dupal signature in the genesis of the Jurassic Ferrar tholeiites from the Prince Albert Mountains, (Victoria Land, Antarctica). *Contributions to Mineralogy and Petrology*, **136**, 1-19.

Baker, M.B., Grove, T.L. and Price, R.C. 1994. Primitive basalts and andesites from the Mt. Shasta region, N. California: products of varying melt fraction and water content. *Contributions to Mineralogy and Petrology*, **118**, 111-129.

Brewer, T. S., Hergt, J. M., Hawkesworth, C. J., Rex D. C. & Storey B. C. 1992. Coats Land dolerites and the generation of Antarctic continental flood basalts. *In:* Storey, B. C., Alabaster, T. & Pankhurst, R. J. (eds) *Magmatism and the causes of Continental Break-Up* Geological Society, London, Special Publications, **64,** 185-208.

Burgess, S.D., Bowring, S.A., Fleming, T.H. & Elliot, D.H. 2015. High-precision geochronology links the Ferrar large igneous province with early-Jurassic ocean anoxia and biotic crisis. *Earth and Planetary Science Letters*, **415**, 90-99.

Coltice, N., Bertrand, H., Rey, P.M., Jourdan, F., Phillips, B.R. & Ricard, Y. 2009. Global warming of the mantle beneath continents back to the Archaean. *Gondwana Research*, **15**, 254-266.

Cox, K.G. & Bristow, J.W. 1984. The Sabine River Basalt Formation of the Lebombo Monocline and south-east Zimbabwe. In: *Petrogenesis of the volcanic rocks of the Karoo province*, A.J. Erlank (ed). Special Publication of the Geological Society of South Africa, **13**, 124-147.

Demarchi, G., Antonini, P., Piccirillo, E.M., Orsi, G., Civetta, L. & D'Antonini, M. 2001. Significance of orthopyroxene and major element constraints on the petrogenesis of Ferrar tholeiites from southern Prince Albert Mountains, Victoria Land, Antarctica. *Contributions to Mineralogy and Petrology*, **142**, 127-146.

Downes, H., Upton, B.G.J., Connolly, J., Beard, A.D. & Bodinier, J-L 2007. Evidence for late Palaeozoic crustal underplating beneath SW Scotland Petrology and geochemistry of a cumulate xenolith suite from Bute. *Journal of the Geological Society, London*, **164**, 1217-1231.

Elliot, D.H. 2013. The geological and tectonic evolution of the Transantarctic Mountains: a review. *In:* Hambrey, M.J., Barker, P.F., Barrett, P.J., Bowman, V., Davies, B., Smellie,

560 J.L. & Tranter, M (eds). *Antarctic Palaeoenvironments and Earth-surface process*.
561 Geological Society London, Special Publications, **381**, 7-35.
562 Elliot, D. H. & Fleming, T. H. 2000. Weddell Triple Junction: The principal focus of Ferrar and
563 Karoo magmatism during the initial break-up of Gondwana. *Geology*, **28**, 539-542.
564 Elliot, D. H. & Fleming, T. H. 2004. Occurrence and Dispersal of Magmas in the Jurassic Ferrar
565 Large Igneous Province, Antarctica. *Gondwana Research*, B, 223-237.
566 Elliot, D.H., Fleming, T.H., Haban, M.A. & Siders, M.A. 1995. Petrology and mineralogy of the
567 Kirkpatrick Basalt and Ferrar Dolerite, Mesa Region, Northern Vitoria Land, Antarctica. *In*:
568 Elliot, D.H. & Blaisdell, L.L. (eds) *Contribution to Antarctic Research IV*. Antarctic
569 Research Series, 67. American Geophysical Union, Washington DC, 103-141.
570 Elliot, D. H., Fleming, T. H., Kyle, P. R. & Foland, K. A. 1999. Long-distance transport of
571 magmas in the Jurassic Ferrar large igneous province, Antarctica. *Earth and Planetary*
572 *Science Letters,* **167**, 89–104.
573 Fleming, T.H., Foland, K.A. & Elliot, D.H. 1995. Isotopic and chemical constraints on the
574 crustal evolution and source signature of Ferrar magmas, north Victoria Land, Antarctica.
575 *Contributions to Mineralogy and Petrology*, **121**, 217-236.
576 Galerne,C.Y., Nuemann, E-R. & Planke, S. 2008. Emplacement mechanisms of sill complexes:
577 Information from the geochemical architecture of the Golden Valley Sill Complex, South
578 Africa. *Journal of Volcanology and Geothermal Research*, **177**, 425-440.
579 Gibson, S.A., Thompson, R.N., Day, J.A., Humphris, S.E. & Dickin A.P. 2005. Melt-generation
580 associated with the Tristan mantle plume: constraints on the origin of EM-1. *Earth and*
581 *Planetary Science Letters*, **237**, 744-767.
582 Greenway, M. E., 1972. The geology of the Falkland Islands. *British Antarctic Survey Scientific*
583 *Reports*, **76**, 42 pp.
584 Harris, C., Marsh, J.S., Duncan, A.R. & Erlank, A.J. 1990. The Petrogenesis of the Kirwan
585 Basalts of Dronning Maud Land, Antarctica. *Journal of Petrology*, **31**, 341-369.
586 Heinonen, J.S. & Luttinen, A.V. 2008. Jurassic dikes of Vestfjella, western Dronning Maud
587 Land, Antarctica: Geochemical tracing of ferropicrite sources. *Lithos*, **105**, 347-364.
588 Heinonen, J.S., Carlson, R.W. & Luttinen, A.V. 2010. Isotopic (Sr, Nd, Pb, and Os) composition
589 of highly magnesian dikes of Vestfjella, western Dronning Maud Land, Antarctica: A key to
590 the origins of the Jurassic Karoo large igneous province? *Chemical Geology*, **277**, 227-244.
591 Heinonen, J.S., Luttinen, A.V., Riley, T.R. & Nichallik, R.M. 2013. Mixed pyroxenite–
592 peridotite sources for mafic and ultramafic dikes from the Antarctic segment of the Karoo
593 continental flood basalt province. *Lithos*, **177**, 266-380.

Heinonen, J.S., Carlson, R.W., Riley, T.R., Luttinen, A.V. & Horan, M.F. 2014. Subduction-modified oceanic crust mixed with a depleted mantle reservoir in the sources of the Karoo continental flood basalt province. *Earth and Planetary Science Letters*, **394**, 229-241.

Hergt J. M., Chappell B. W., Mcculloch M. T., McDougall I. & Chivas A. R. 1989. The geochemistry of Jurassic dolerites from Portal Peak, Antarctica. *Contributions to Mineralogy and Petrology*, **102**, 298-305.

Herzberg, C. & Asimow, P.D. 2008. Petrology of some oceanic island basalts: PRIMELT2.XLS software for primary magma calculation. *Geochemistry, Geophysics, Geosystems*, **9**.

Herzberg, C. & Gazel, E. 2009. Petrological evidence for secular cooling in mantle plumes. *Nature*, **458**, 619-623.

Hole, M.J. 2015. The generation of continental flood basalts by decompression melting of internally heated mantle. *Geology*, **43**.311-314.

Hole M.J. & Morrison, M.A. 1992. The differentiated boss Cnoc Rhaonastil, Islay; a natural experiment in the low pressure differentiation of an alkali olivine-basalt magma. *Scottish Journal of Geology*, **28**, 55-69.

Hole, M.J., Millett, J.M., Rogers, N.W. & Jolley, D.W. 2015. Rifting and mafic magmatism in the Hebridean basins. *Journal of the Geological Society, London,* **172**, 218-236.

Jourdan F., Bertrand H., Schärer U., Blichert-Toft J., Feraud G. & Kampunzu A.B. 2007b. Major and trace element and Sr, Nd, Hf, and Pb isotope compositions of the Karoo large igneous province, Botswana-Zimbabwe: lithosphere *vs* mantle plume contribution. *Journal of Petrology*, **48**, 1043-1077

Keiding, J.K., Trumbull, R.B., Veksler, I.V. & Jerram, D.A. 2011. On the significance of ultra-magnesian olivines in basaltic rocks. *Geology*, **39**, 1095-1098.

Lambart, S., Lapporte, D. & Schiano, P. 2013. Markers of the pyroxenite contribution in the major-element compositions of oceanic basalts: Review of the experimental constraints. *Lithos*, **160-161**, 14-36.

Luttinen, A.V. & Furnes, H., 2000. Flood basalts of the Vestfjella: Jurassic magmatism across an Arcehan-Proterozoic lithospheric boundary in Dronning Maud Land, Antarctica. *Journal of Petrology*, **41**, 1271-1305.

Luttinen, A.V., Ramo, O.T. & Huhma, H. 1998. Neodymium and strontium isotope and trace element composition of a Mesozoic CFB suite from Dronning Maud Land, Antarctica: implications for lithosphere and asthenosphere contributions to Karroo magmatism. *Geochimica et Cosmochimica Acta*, **15**, 2701-2714.

627 Macdonald, D.I.M., Gomez-Perez, I., Franzese, J., Spalleti, L., Lawver, L., Gahagan, L.,
628 Dalziel, I.W.D., Thomas, C.J., Trewin, N.H., Hole, M.J. & Paton, D. 2003. Mesozoic break-
629 up of SW Gondwana: implications for regional hydrocarbon potential of the southern South
630 Atlantic. *Marine & Petroleum Geology*, **20**, 287-308
631 Marsh, J.S., Hooper, P.R., Rehacek, J., Duncan, R.A. & Duncan, A.R. 1997. Stratigraphy and
632 age of Karroo basalts of Lesotho and implications for correlations within the Karroo
633 Igneous Province. In: Mahoney, J.J. & Coffin, M.F. (eds*) Large Igneous Provinces*, A G U
634 Geophysical Monographs, 100, 247-272.
635 McClintock, M., Marsh, J. & White, J.D.L. 2008. Compositionally diverse magmas erupted
636 close together in space and time within a Karoo flood basalt crater complex. *Bulletin of*
637 *Volcanology*, **70**, 923-946.
638 Mitchell, C., Ellam, R.M. & Cox, K.G. 1999. Mesozoic dolerite dykes of the Falkland Islands:
639 petrology, petrogenesis and implications for geochemical provinciality in Gondwanaland
640 low-Ti basaltic rocks. *Journal of the Geological Society, London,* **156**, 901-916.
641 Mitchell, C., Taylor, G.K., Cox, K.G. & Shaw, J. 1986. Are the Falkland Islands a rotated
642 microplate? *Nature*, **319**, 131-134.
643 Molzahn, M., Reisberg, L. & Wörner, G. 1996. Os, Sr, Nd, Pb, O isotope and trace element
644 data from the Ferrar flood basalts, Antarctica: evidence for an enriched subcontinental
645 lithospheric source. *Earth and Planetary Science Letters*, **144**, 529-546.
646 Muirhead, J.D., Airoldi, G., White, J.L. and Rowland, J.V. 2014. Cracking the lid: Sill-fed
647 dikes are the likely feeders of flood basalt eruptions. *Earth and Planetary Science Letters*,
648 **406**, 187-197.
649 Mussett, A.E. & Taylor, G.K. 1994. ^{40}Ar-^{39}Ar ages for dykes from the Falkland Islands with
650 implications for the break-up of southern Gondwanaland. *Journal of the Geological Society,*
651 *London,* **151**, 79-81.
652 Nuemann, E-R., Svensen, H., Galerne, G.Y. & Planke, S. 2011. Multistage Evolution of
653 Dolerites in the Karoo Large Igneous Province, Central South Africa. *Journal of Petrology*,
654 **52**, 959-984.
655 Putirka, K.D., Perfit, M., Ryerson, F.J. & Jackson, M.G. 2007. Ambient and excess mantle
656 temperatures, olivine thermometry, and active vs. passive upwelling. *Chemical Geology*, **241**,
657 177-206.
658 Richards, P.C., Stone, P., Kimbell, G.S., Mcintosh, W.C. & Phillips, E.R. 2013. Mesozoic
659 magmatism in the Falkland Islands (South Atlantic) and their offshore sedimentary basins.
660 *Journal of Petroleum Geology*, **36**, 61-74.

661 Riley, T.R., Curtis, M.L., Leat, P.T., Watkeys, M.K., Duncan, R.A., Millar, I.L. & Owens, W.H.
662 2006. Overlap of Karoo and Ferrar Magma Types in KwaZulu-Natal, South Africa.
663 *Journal of Petrology*, **47**, 541-566.
664 Sato, M., Shuto, K., Nohara-Imanaka, R., Takazawa, E., Osanai, Y. & Nakano, N. 2014.
665 Repeatedmagmatism at 34 Ma and 23-20 Ma producing highmagnesian adakitic andesites
666 and transitional basalts on southern Okushiri Island, NE Japan arc. *Lithos*, **205**, 60-83.
667 Sushchevskaya, N.M., Korago, E.A., Belyatsky, B.V. & Sirotkin, A.N. 2009. Evolution of the
668 Karoo-Maud mantle plume in Antarctica and its influence on the magmatism of the early
669 stages of Indian ocean opening. *Geochemistry International*, **47**, 1-17.
670 Stone, P., Kimbell, G.S. & Richards, P.C. 2009. Rotation of the Falklands microplate reassessed
671 after recognition of discrete Jurassic and Cretaceous dyke swarms. *Petroleum Geoscience*,
672 **15**, 279-287.
673 Stone, P., Richards, P.C., Kimbell, G.S., Esser, R.P.,& Reeves, D. 2008 Cretaceous dykes
674 discovered in the Falkland Islands: implications for regional tectonics in the South Atlantic.
675 *Journal of the Geological Society, London,* **165**, 1-4
676 Storey, B.C., Alabaster, T., Hole, M.J., Pankhurst, R.J. & Wever, H. 1992. Role of subduction-
677 plate boundary forces during the initial stages of Gondwana break-up: Evidence from the
678 proto-Pacific margin of Antarctica. *In:* Storey, B. C., Alabaster, T. & Pankhurst, R. J. (eds)
679 *Magmatism and the causes of Continental Break-Up* Geological Society, London, Special
680 Publications, **64,** 149-163.
681 Sweeney R. J., Duncan A. R., Erlank A. J. 1994. Geochemistry and Petrogenesis of Central
682 Lebombo basalts of the Karoo igneous province. *Journal of Petrology*, **35** 95-125.
683 Sun, S-S. & Mcdonough, W. F. 1989. Chemical and isotopic systematics of oceanic basalts:
684 implications for mantle composition and processes. In: Saunders, A.D. & Norry, M.J.,
685 (eds). *Magmatism in the ocean basins*. Geological Society, London, Special Publications,
686 **42,** 313-345.
687 Sushchevskaya, N. M., Belyatskii, B. V., Leichenov, G. L. & Laiba A. A. 2009. Evolution of the
688 Karoo-Maud plume in Antarctica and its influence on the magmatism of the early stages of
689 Indian Ocean opening. *Geochemistry International*, **47**, 1-17
690 Svensen, H., Corfu, F., Polteau, S., Hammer, O & Planke, S. 2012. Rapid magma emplacement
691 in the Karoo Large Igneous Province. *Earth and Planetary Science Letters*, **325-326**, 1-9.
692 Taylor, G.K. & Shaw, J. 1989. The Falkland Islands: New Palaeomagnetic Data and their Origin
693 as a Displaced Terrane from Southern Africa, In: J.W. Willhouse (ed), Deep Structure and
694 Past Kinematics of Accreted Terranes, AGU Monographs 50, vol. 5, pp. 59-72 Washington

695 Thistlewood, L., Leat, P. T., Millar, I.L., Storey, B.C. & Vaughan, A. P. M. 1997. Basement
696 Geology and Palaeozic-Mesozoic mafic dykes from the Cape Meredith Complex, Falkland
697 Islands: a record of repeated intracontinental extension. *Geological Magazine,* **134**, 355-
698 367.
699 Thompson, R.N., Gibson, S.A., Dickin, A.P. & Smith, P.M. 2001. Early Cretaceous basalt and
700 picrate dykes of the Southern Etendeka region, NW Namibia: windows into the role of the
701 Tristan plume in Parana-Etendeka magmatism. *Journal of Petrology*, **42**, 2049-2081.
702 Trewin, N.H., Macdonald, D.I.M., & Thomas, C.G.C. 2002. Stratigraphy and sedimentology of
703 the Permian of the Falkland Islands: lithostratigraphic and palaeoenvironmental links with
704 South Africa. *Journal of the Geological Society, London,* **159**, 5–19.
705 Villiger, S., Ulmer, P. & Muntener, O. 2007. Equilibrium and fractional crystallization
706 experiments at 0.7 GPa; the effect of pressure on phase relations and liquid compositions of
707 tholeiitic magmas. *Journal of Petrology*, **48**, 159-184.
708 Wilhelm, S. & Wörner, G. 1996. Crystal size distribution in Jurassic Ferrar flows and sills
709 (Victoria Land, Antarctica): evidence for processes of cooling, nucleation and
710 crystallization. *Contributions to Mineralogy and Petrology*, **125**, 1-15.
711 Williamson, I.T. & Bell, B.R. 2012. The Staffa Lava Formation: graben-related volcanism,
712 associated sedimentation and landscape character during the early development of the
713 Palaeogene Mull Lava Field, NW Scotland. *Scottish Journal of Geology*, **48**, 1-46.
714

Figure Captions

Figure 1. a) Reconstruction of Southern Gondwana showing the position of the Falkland Islands relative to south-eastern Africa prior to continental break-up. The three arrows represent the main dyke trends on the Falkland Islands rotated back to their pre-180 Ma orientation. After Trewin *et al.* (2002). b) Southern Gondwana, in the Middle Jurassic, showing the distribution of Jurassic break-up related magmas in southern Africa and Antarctica. MEB, Maurice Ewing Bank; EWM, Ellsworth-Whitmore Mountains; AP, Antarctic Peninsula; SA, South Africa; SAM, South America; ANT, Antarctica. Position of the Weddell, Limpopo and Lower Zambesi triple junctions are from Elliot & Fleming (2000). Ar-Ar ages, this study and Stone *et al.* (2009). After Macdonald *et al.* (2003). Key to shading for Fig. 1b is the same as that for Fig. 1a.

Figure 2. Map of the Falkland Islands showing the distribution of magnetic anomalies and main trends of dyke swarms. Solid or pecked lines do not necessarily represent continuous exposure of dykes. Inset; azimuths of Dykes in the South Harbour area of West Falkland. The rectangle at South Harbour is the area covered by the map in the supplementary material, which gives the sample locations and geochenmical type to which the dykes belong in that area. After Stone *et al.* (2009) and Richards *et al.* (2013). Ar-Ar ages (this study, Stone *et al.* 2008; 2009) and sample locations which are mentioned in the text, are indicated, along with the geochemical group to which the intrusions belong, given by the following abbreviations; PST, Port Sussex Type; MAT, Mount Alice Type, E-W, East-West Type of Mitchell *et al.* (1999); DIT, Dyke Island Type. Identifying characteristics of each type of intrusion are discussed in detail in the text.

Figure 3. Ar-Ar step-heating spectrum for plagioclase in sample WI-5. Full data are given in the supplementary materials.

Figure 4. Major (wt%) and trace element (in ppm) variations *versus* MgOwt% in Falkland Islands dykes. Filled dots, Port Sussex Creek type (PST) NE-SW two-pyroxene dolerites; open triangles, E-W olivine dolerite dykes; open squares, Lively Island dyke; filled squares, Mount Alice-type (MAT) dykes; open dots, low TiO_2 DIT intrusions; filled diamonds, high TiO_2 DIT intrusions; open diamonds, evolved sheets from the South Harbour-Dyke Island transect (Dyke Island Type; DIT); crosses, Pony's Pass N-S Cretaceous dyke (Stone *et al.* 2008). Data from this study, Mitchell *et al.* (1999) and Thistlewood *et al.* (1997).

Figure 5. Pyroxene end-member compositions represented in the quadrilateral system Enstatite - Ferrosilite – Wollastonite for Falkland Islands intrusions (this study and Mitchell *et al.* 1999) and dolerites from the Transantarctic Mountains (Elliot 1995; Demarchi *et al.* 2001). MFCT,

748 Mount Fazio Chemical Type; SPCT, Scarab Peak Chemical Type; NVL, Northern Victoria
749 Land.

750 Figure 6. Chondrite-normalized REE profiles for representative samples of a) DIT intrusions
751 and b) PST, MAT and E-W intrusions.

752 Figure 7. a) to d) Multi-element ORB-normalized (Sun & McDonough 1989) variation diagrams
753 for Falkland Islands dykes. Comparable basalts from other regions of the low TiO_2 Gondwana
754 LIP are shown by grey lines. Sample SA.6.1 (South Africa), Riley *et al.* (2006); VF111-85, CT3
755 basalt, Dronning Maud Land (Luttinen & Furnes 2000); 47206-3, low TiO_2 tholeiite from
756 Schirmacher Oasis, Dronning Maud Land (Sushchevskaya *et al.* 2009); Average MFCT from
757 Elliot *et al.* (1995).

758 Figure 8. a) εNd_{182} *versus* $^{87}Sr/^{86}Sr_{182}$; b) $^{207}Pb/^{204}Pb$ *versus* $^{206}Pb/^{204}Pb$ for Falkland Islands
759 dykes. c) εNd_{182} *versus* $^{207}Pb/^{204}Pb$ for Falkland Islands intrusions. Symbols as for Fig. 4. Data
760 sources this study, Mitchell *et al.* (1999) and Thistlewood *et al.* (1997).

761 Figure. 9 a) εNd_{182} *versus* MgO; b) εNd_{182} versus Th/Ta and c) $^{87}Sr/^{86}Sr_{182}$ *versus* 1/Sr for
762 Falkland Islands intrusions. Symbols as for Fig. 4 except grey dots are for the lowest reported
763 Th/Ta for Ferrar dolerites (Fleming *et al.* 1995). Parameters for the AFC mixing line are given
764 in Table 4 with % AFC given on the mixing line.

765 Figure 10. Ti/Zr *versus* SiO_2 for Falkland Islands dykes. Symbols as for Fig. 4.

766 Figure 11. TiO_2 *versus* MgO, for Falkland Islands dykes the Ferrar LIP and igneous rocks
767 considered to be transitional between the compositions of Ferrar and Karoo magmas. Data
768 sources; Hergt *et al.* (1989), Brewer *et al.* (1992), Elliot *et al.* (1995), Fleming *et al.* (1995),
769 Molzahn *et al.* (1996), Wilhelm & Worner (1996), Antonini *et al.* (1999), Elliot *et al.* (1999),
770 Elliot & Fleming (2004), Riley *et al.* (2006). Falkland Islands samples symbols as for Fig. 4.

771 Fig. 12. εNd_{182} *versus* $^{87}Sr/^{86}Sr_{182}$ for Falkland Islands PST intrusions (filled dots) Karoo low
772 TiO_2 volcanic rocks (open circles), Dronning Maud Land CT1 (open triangles), CT2 (filled
773 diamonds) and CT3 (filled triangles) basalts. Details of the parameters used in generating the
774 three AFC mixing lines (CT1, PST-1 and PST-2) are given in Table 4. Each cross represents 1%
775 AFC. Data sources for Karoo Province; Galerne *et al.* (2008); McClintock *et al*. (2008);
776 Neumann *et al.* (2011).

777 Figure 13. a) CaO *versus* MgO (weight %) for Falkland Islands intrusions (black dots PST; grey
778 dots, DIT; grey squares MAT; triangles, E-W) and Dronnning Maud Land high MgO, silica-

779 oversaturated CT1 basalts (circles). The dividing line between melts derived from peridotite
780 and pyroxenite sources is taken from Herzberg & Asimow (2008). Lines with crosses and
781 arrows represent the effect of accumulation of the phase indicated on the composition of PST
782 basalt NEF9, with each cross representing 5% accumulation. b) Cr (ppm) *versus* SiO_2 for
783 Falkland Islands intrusions (symbols as for Fig. 4) and high-Mg andesites from Mt Shasta
784 (crosses; Baker *et al.* 1994).

785 Figure 14. Ti/Zr *versus* SiO_2, for a) Karoo LIP volcanic rocks and b) Ferrar LIP volcanic rocks.
786 Note that the KwaZulu-Natal and Theron Mountains low TiO_2 samples are considered to be
787 magma types transitional between Karoo and Ferrar types. Data sources; Transantarctic
788 Mountains and Theron Mountains; Hergt *et al.* (1989), Brewer *et al.* (1992), Elliot *et al.* (1995),
789 Fleming *et al.* (1995), Molzahn *et al.* (1996), Wilhelm & Worner (1996), Antonini *et al.* (1999),
790 Elliot *et al.* (1999), Elliot & Fleming (2004). Karoo (including Dronning Maud Land) Luttinen
791 *et al.* (1998), Luttinen & Furnes (2000), Heinonen & Luttinen (2008), Heinonen *et al.* (2010;
792 2013; 2014) Neumann *et al*. (2011). Kirwanveggan; Harris *et al.* (1990).

793 Figure 15. a) Olivine equilibration temperatures (°C) *versus* Mg# of liquid in equilibrium with
794 olivine for Ahlmannryggen dykes (filled dots; Heinonen & Luttinen 2008), Vestfjella high TiO_2
795 ferropicrite (filled triangles; Heinonen *et al.* 2013), Etendeka picrite (open squares; Kieding *et*
796 *al.* 2011) and Falklands Islands MAT intrusion (star in circle) and E-W intrusions (open
797 triangles). Olivine equilibration temperatures have been calculated according to the scheme of
798 Putirka *et al*. (2007). Vertical lines connecting points for Ahlmannryggen samples are calculated
799 equilibration temperatures for different olivine phenocrysts in individual whole-rock samples.
800 Figures in italics are T_P from melt inclusions for Etendeka samples plotted in Fig. 15a (Kieding
801 *et al.* 2011). b) Inferred temperature-pressure conditions at which fractional melting terminated
802 for calculated primary magmas from Dronning Maud Land, the Karoo Province of southern
803 Africa, Ferrar dolerites of Antarcitca and picrites of the Etendeka Province of western Africa.
804 The diagram was constructed following the methods of Herzberg and Gazel (2009) with data for
805 the Ferrar province and Iceland from Hole (2015). Samples with MgO > 20 weight % are
806 shown schematically following an adiabatic pathway for T_P = 1640°C. The diagonally shaded
807 box on the temperature axis is the range of olivine equilibration temperatures, calculated at 0
808 GPa, for olivine in ferro-picrite dykes from Dronning Maud following the method of Putirka et
809 al. (2007), and the box labelled 'MAT & E-W' is the same calculations for MAT and E-W
810 intrusions. Adiabatic melting paths are labelled with mantle potential temperature. 2σ error bars
811 are from Hole (2015). c) T_P calculated from melt inclusions in ultra-magnesian olivines from the

812 Etendeka Provice *versus* olivine equilibration temperatures for the same samples. Data from
813 Keiding *et al.* (2011).

814

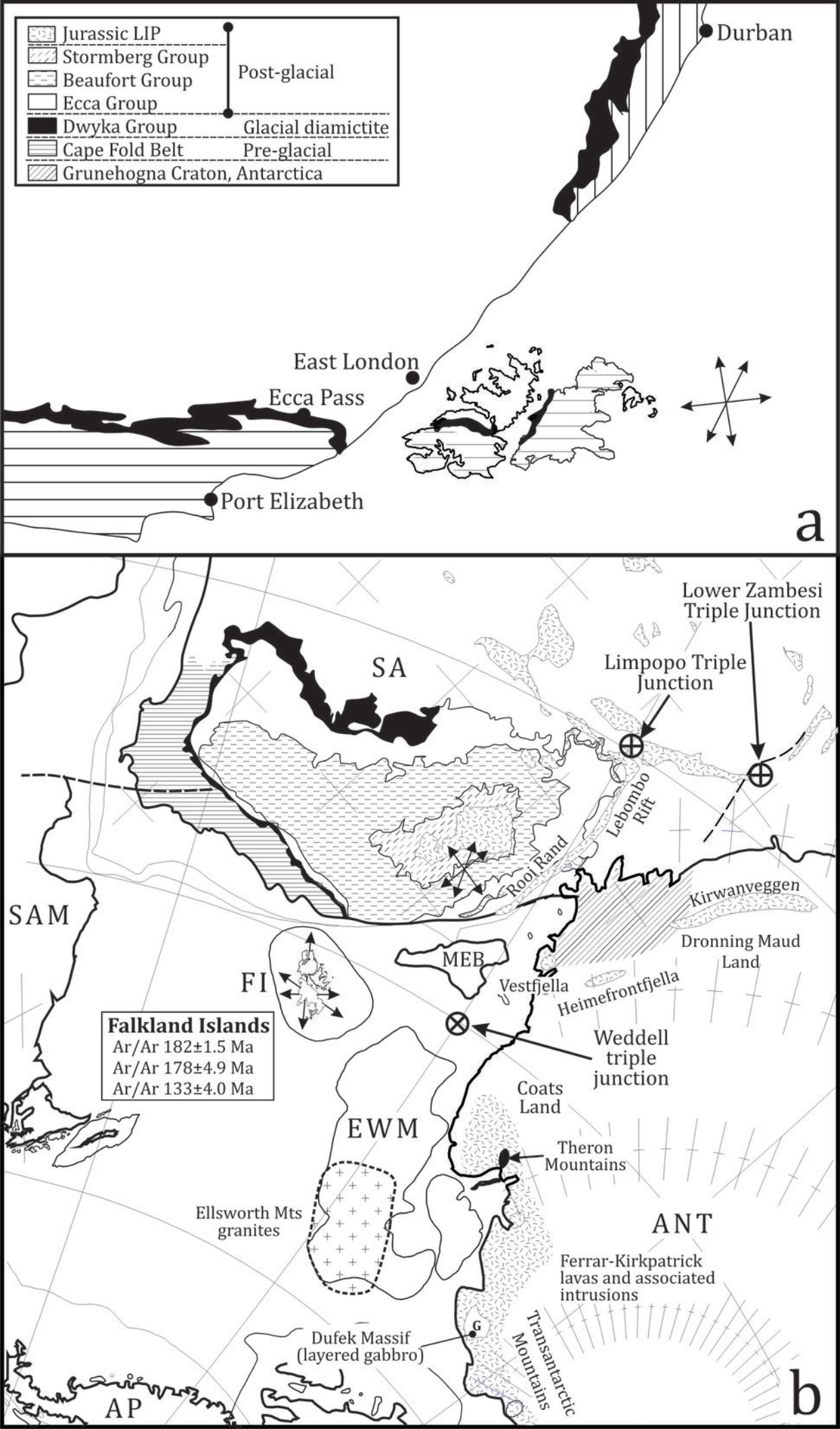
Jurassic LIP
Stormberg Group
Beaufort Group
Ecca Group
Post-glacial
Dwyka Group
Glacial diamictite
Cape Fold Belt
Pre-glacial
Grunehogna Craton, Antarctica
Durban
East London
Ecca Pass
Port Elizabeth
a
Lower Zambesi Triple Junction
Limpopo Triple Junction
SA
Lebombo Rift
Rooi Rand
Kirwanveggen
Dronning Maud Land
SAM
MEB
FI
Vestfjella
Heimefrontfjella
Falkland Islands
Ar/Ar 182±1.5 Ma
Ar/Ar 178±4.9 Ma
Ar/Ar 133±4.0 Ma
Weddell triple junction
Coats Land
EWM
Theron Mountains
Ellsworth Mts granites
ANT
Ferrar-Kirkpatrick lavas and associated intrusions
Dufek Massif (layered gabbro)
Transantarctic Mountains
AP
b

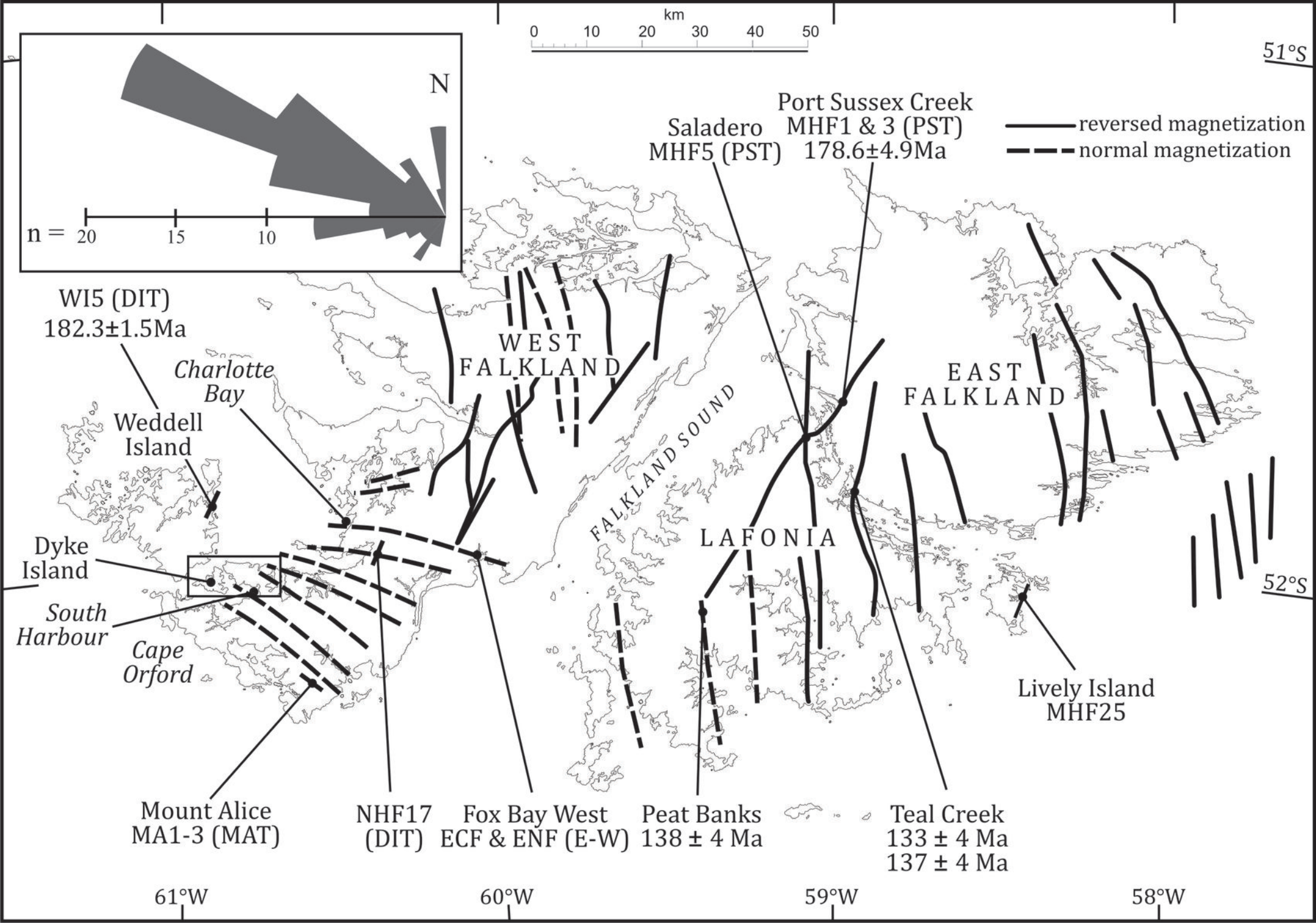
km
0
10
20
30
40
50
N
n =
20
15
10
51°S
52°S
61°W
60°W
59°W
58°W
reversed magnetization
normal magnetization
Port Sussex Creek
MHF1 & 3 (PST)
178.6±4.9Ma
Saladero
MHF5 (PST)
WI5 (DIT)
182.3±1.5Ma
Charlotte
Bay
Weddell
Island
WEST
FALKLAND
FALKLAND SOUND
EAST
FALKLAND
LAFONIA
Dyke
Island
South
Harbour
Cape
Orford
Lively Island
MHF25
Mount Alice
MA1-3 (MAT)
NHF17
(DIT)
Fox Bay West
ECF & ENF (E-W)
Peat Banks
138 ± 4 Ma
Teal Creek
133 ± 4 Ma
137 ± 4 Ma

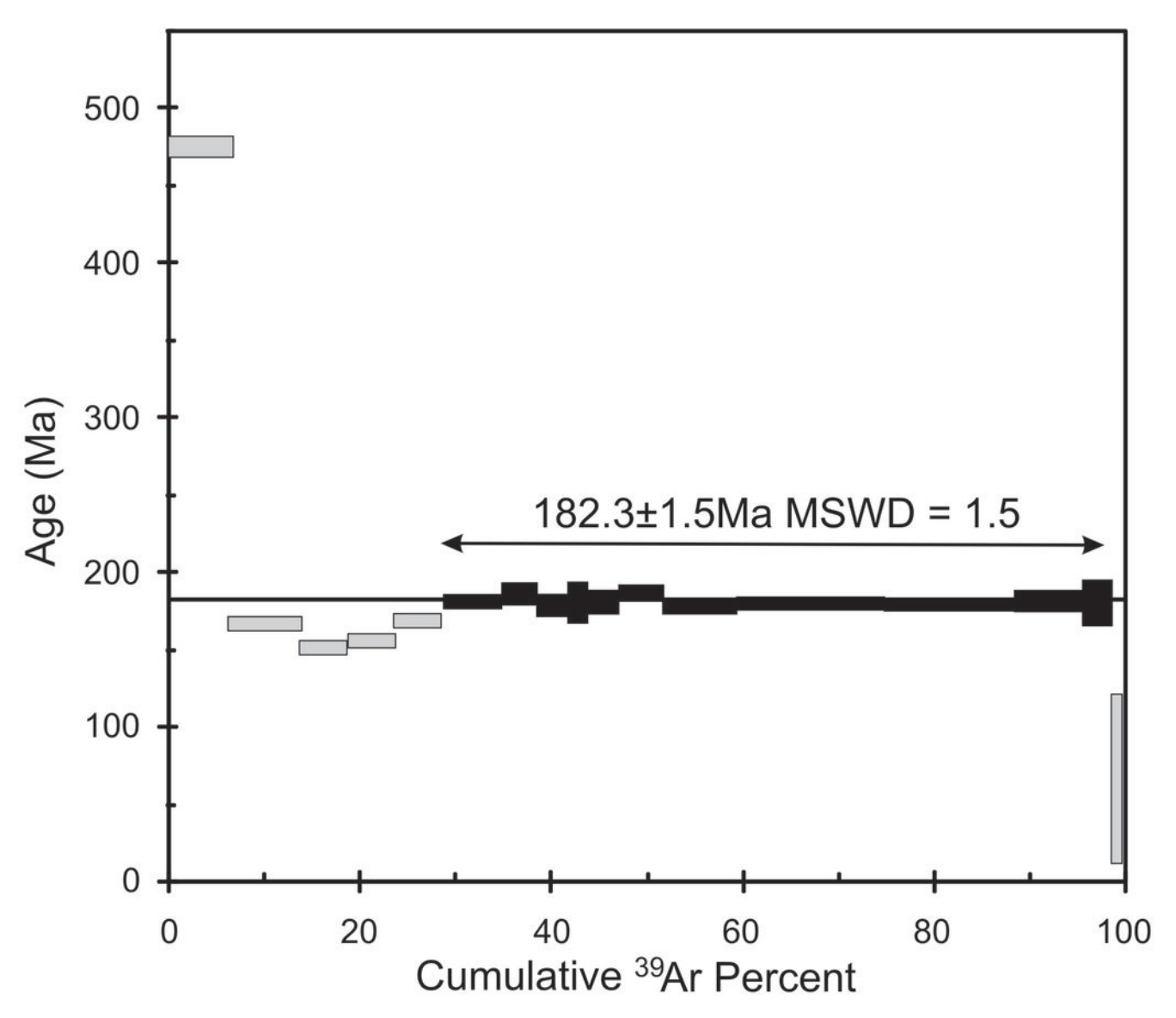
500
400
300
200
100
0
Age (Ma)
182.3±1.5Ma MSWD = 1.5
0
20
40
60
80
100
Cumulative 39Ar Percent

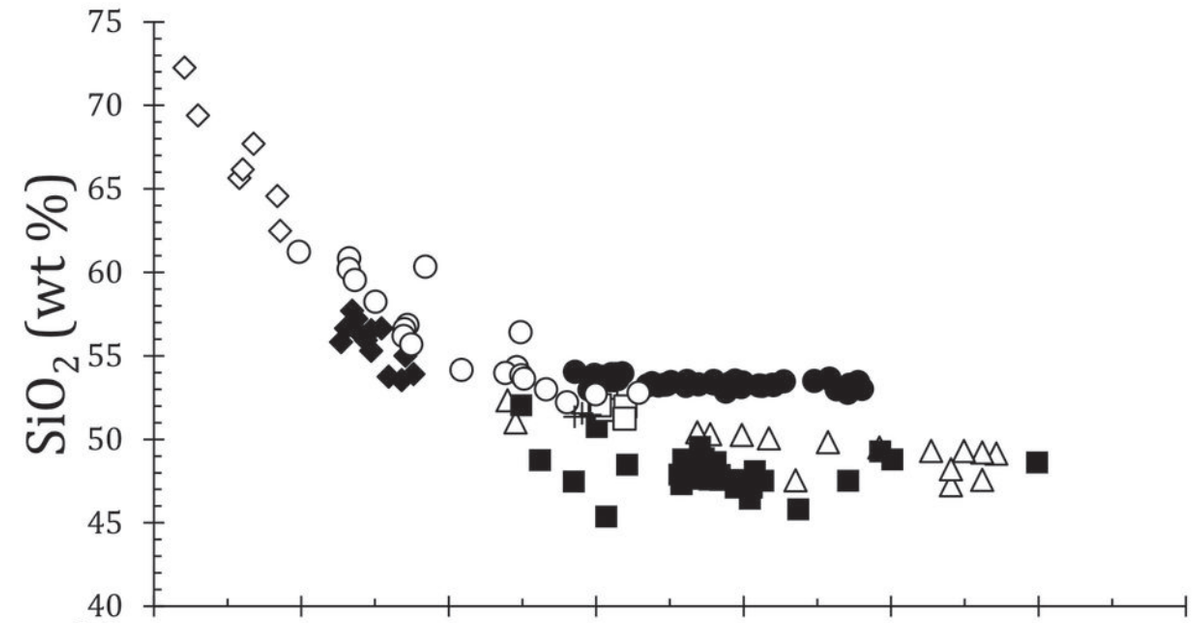
SiO2 (wt %)
75
70
65
60
55
50
45
40

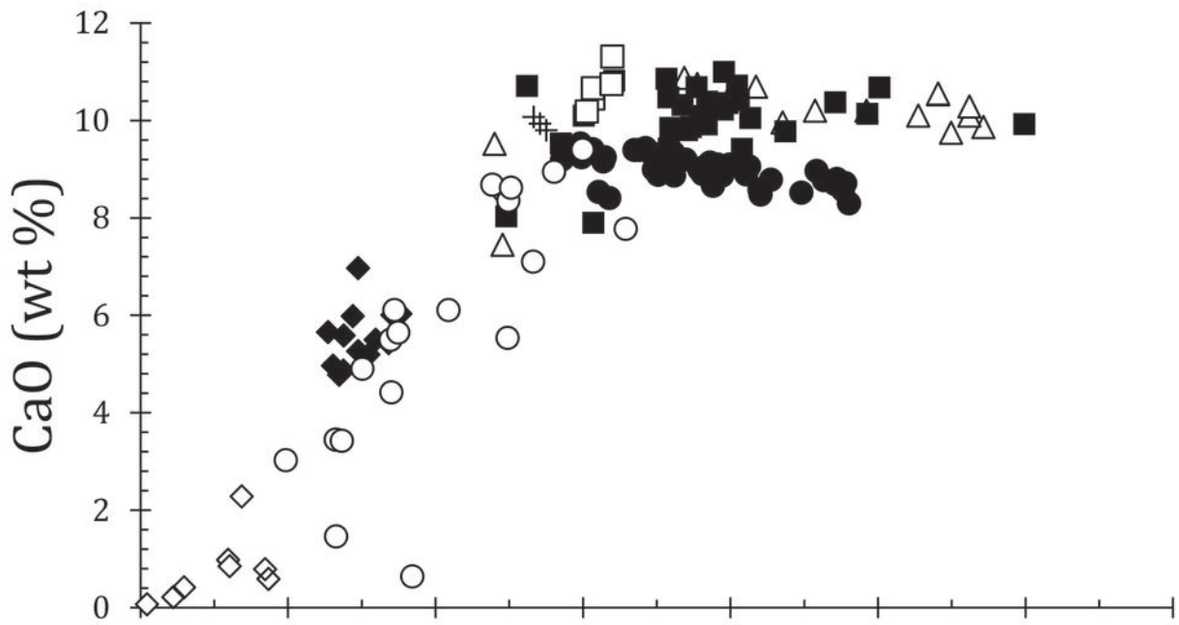
CaO (wt %)
12
10
8
6
4
2
0

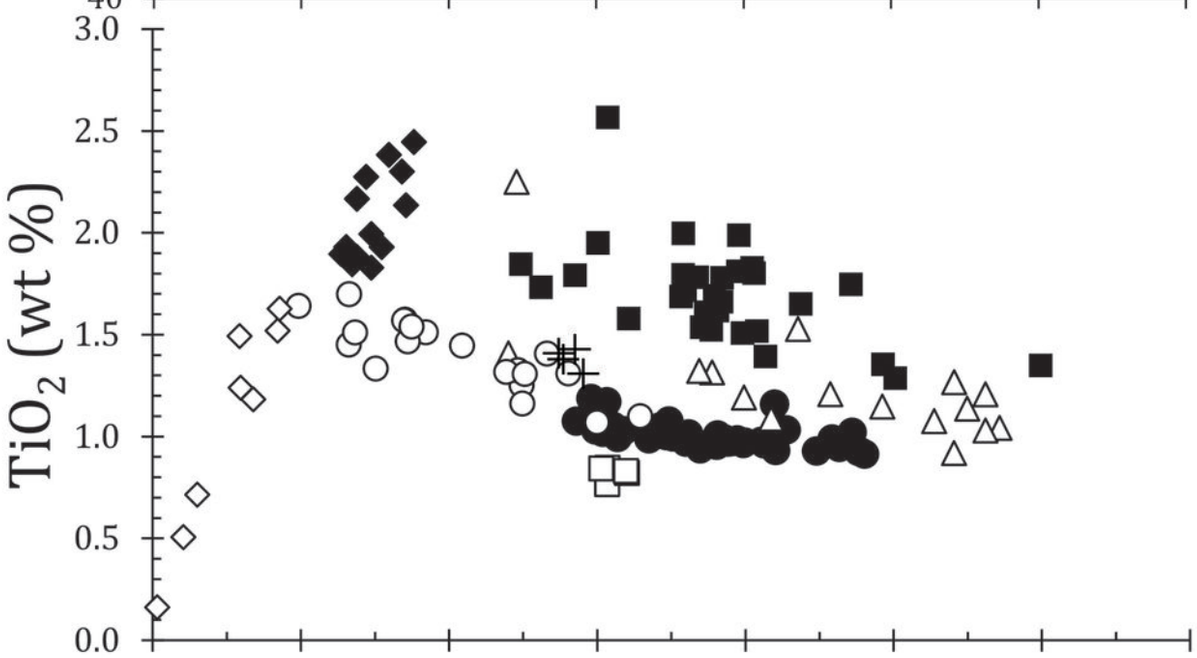
TiO2 (wt %)
3.0
2.5
2.0
1.5
1.0
0.5
0.0

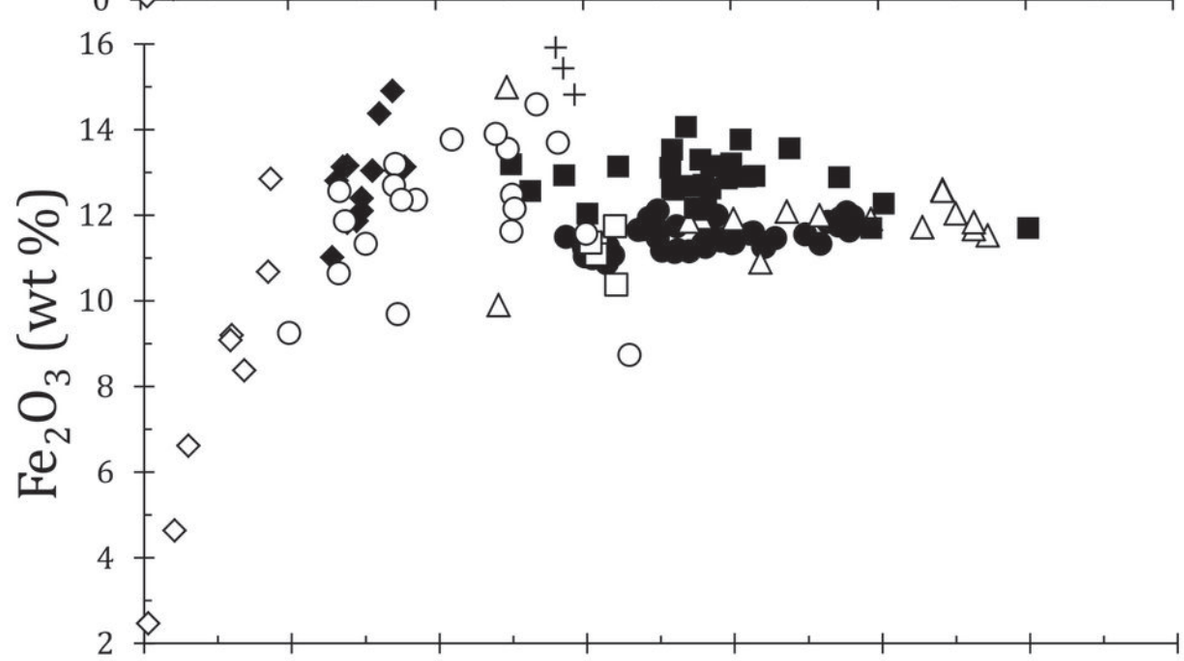
Fe2O3 (wt %)
16
14
12
10
8
6
4
2

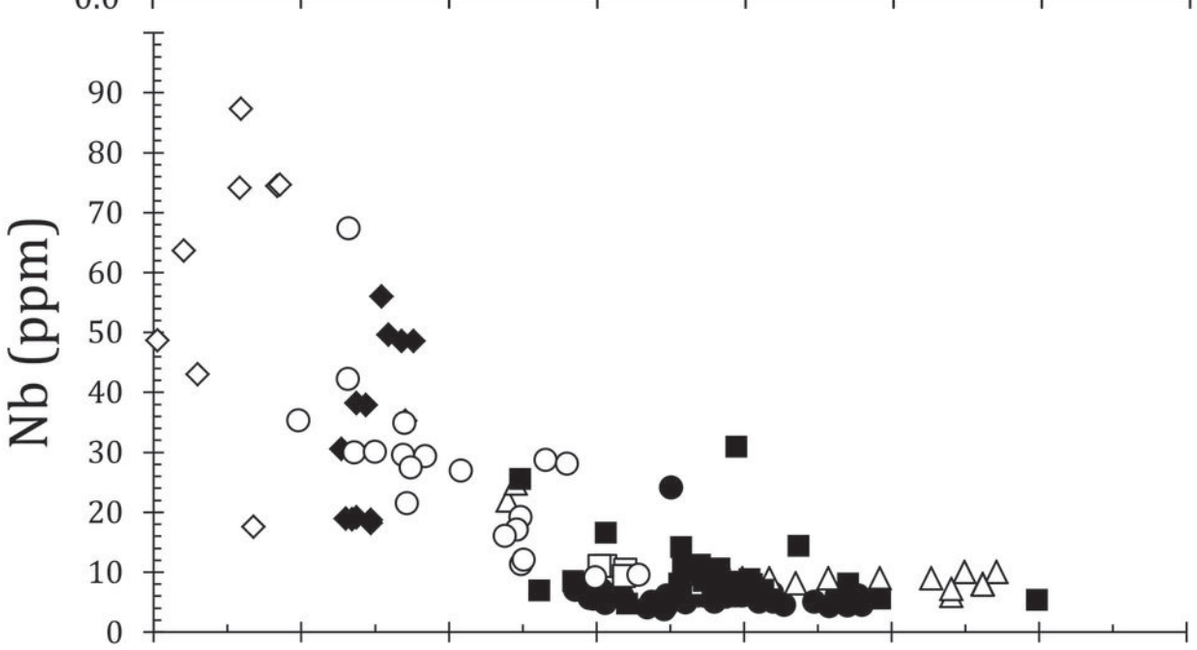
Nb (ppm)
90
80
70
60
50
40
30
20
10
0

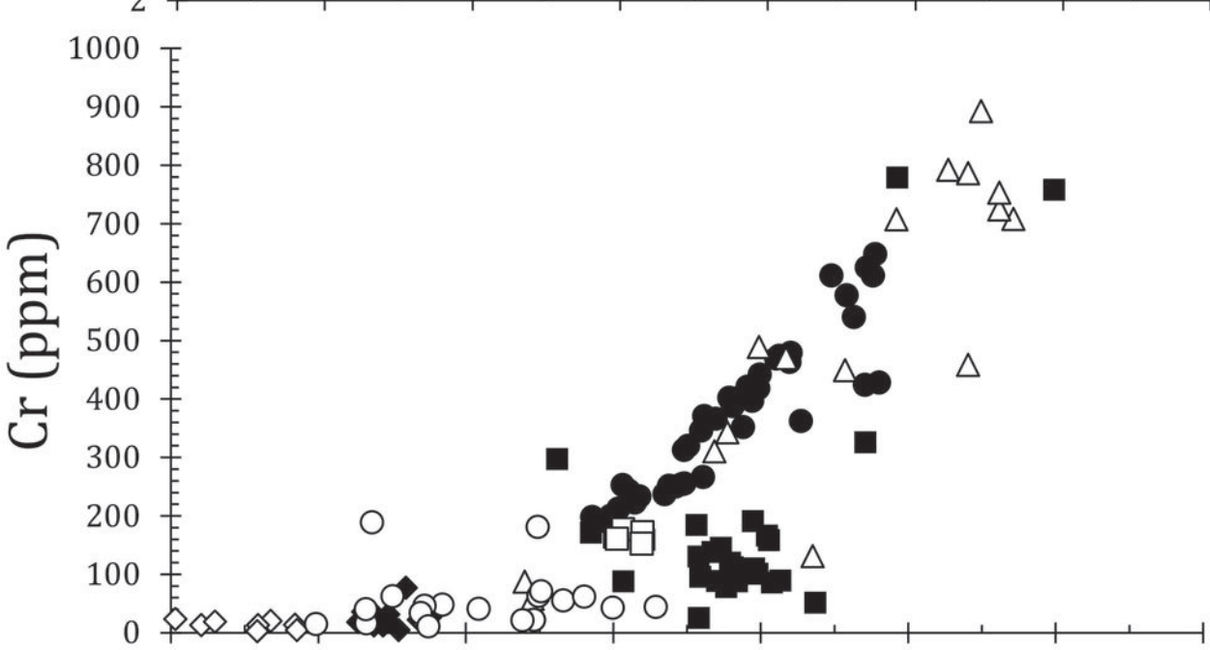
Cr (ppm)
1000
900
800
700
600
500
400
300
200
100
0

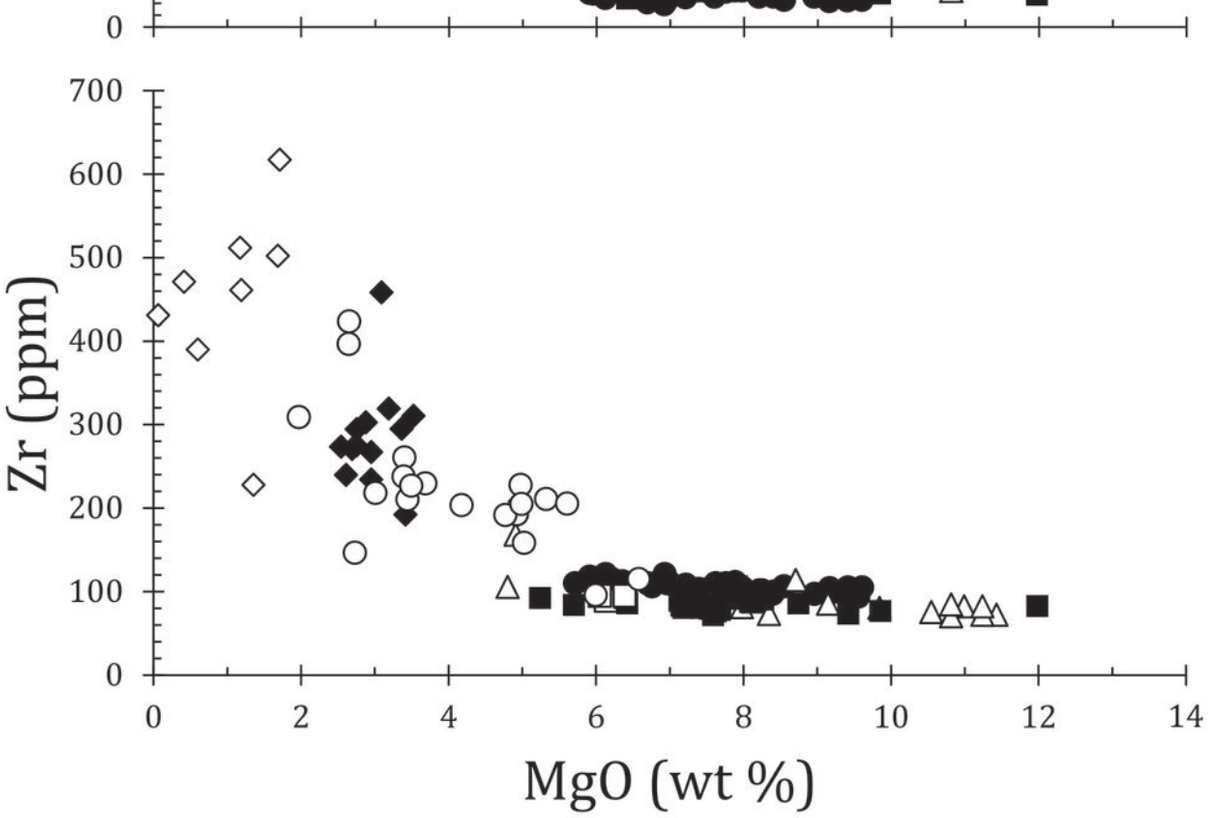
Zr (ppm)
700
600
500
400
300
200
100
0
0
2
4
6
8
10
12
14
MgO (wt %)

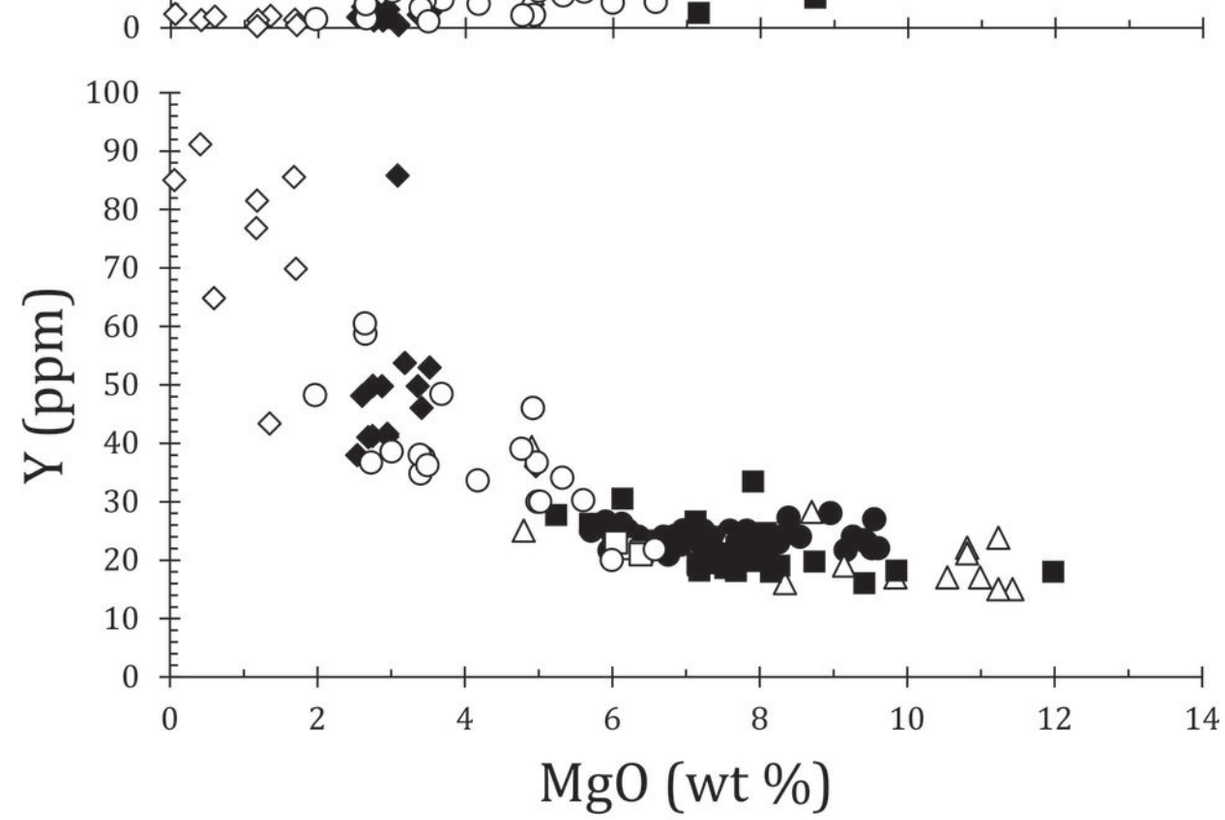
Y (ppm)
100
90
80
70
60
50
40
30
20
10
0
0
2
4
6
8
10
12
14
MgO (wt %)

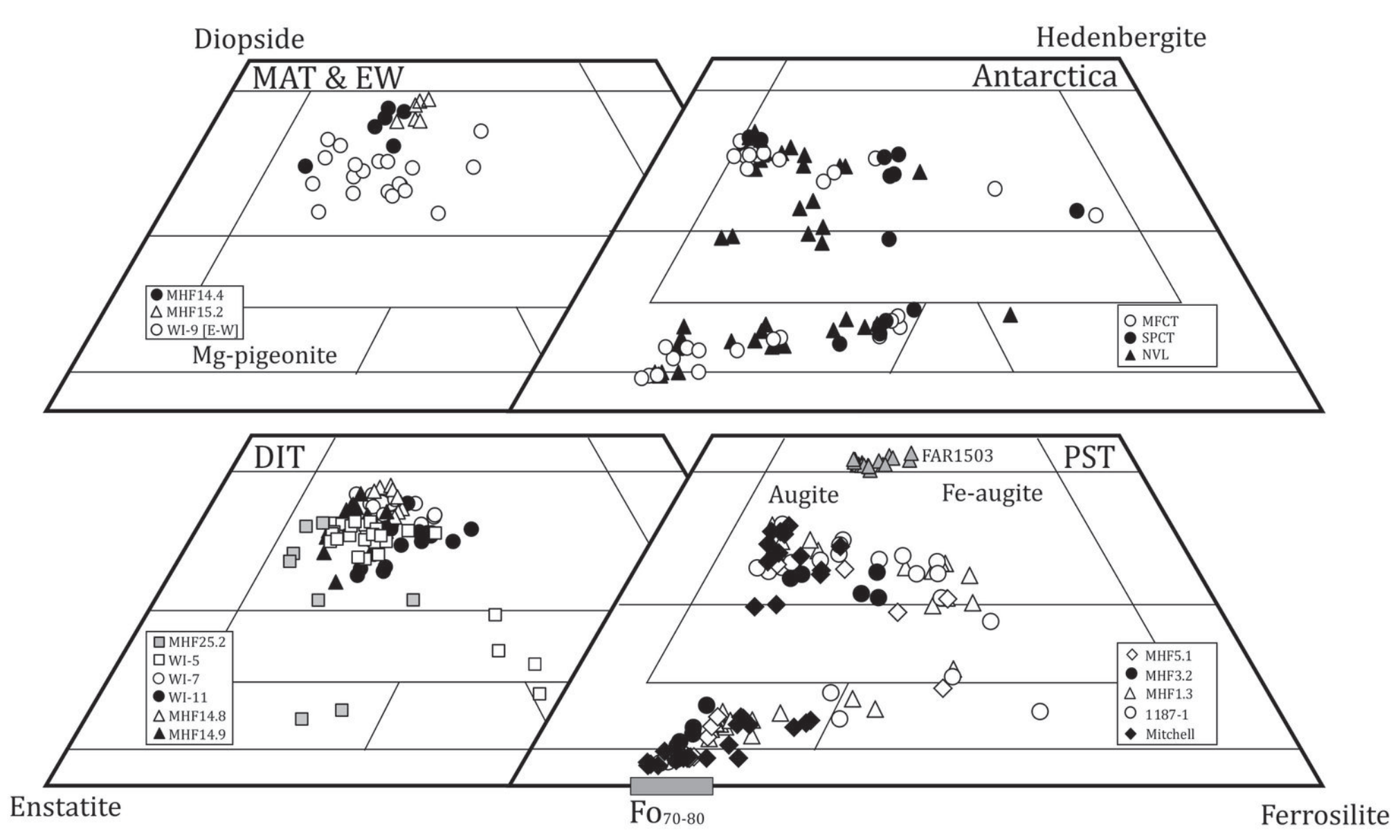
Diopside
Hedenbergite
MAT & EW
Antarctica
MHF14.4
MHF15.2
WI-9 [E-W]
Mg-pigeonite
MFCT
SPCT
NVL
DIT
FAR1503
PST
Augite
Fe-augite
MHF25.2
WI-5
WI-7
WI-11
MHF14.8
MHF14.9
MHF5.1
MHF3.2
MHF1.3
1187-1
Mitchell
Enstatite
Fo70-80
Ferrosilite

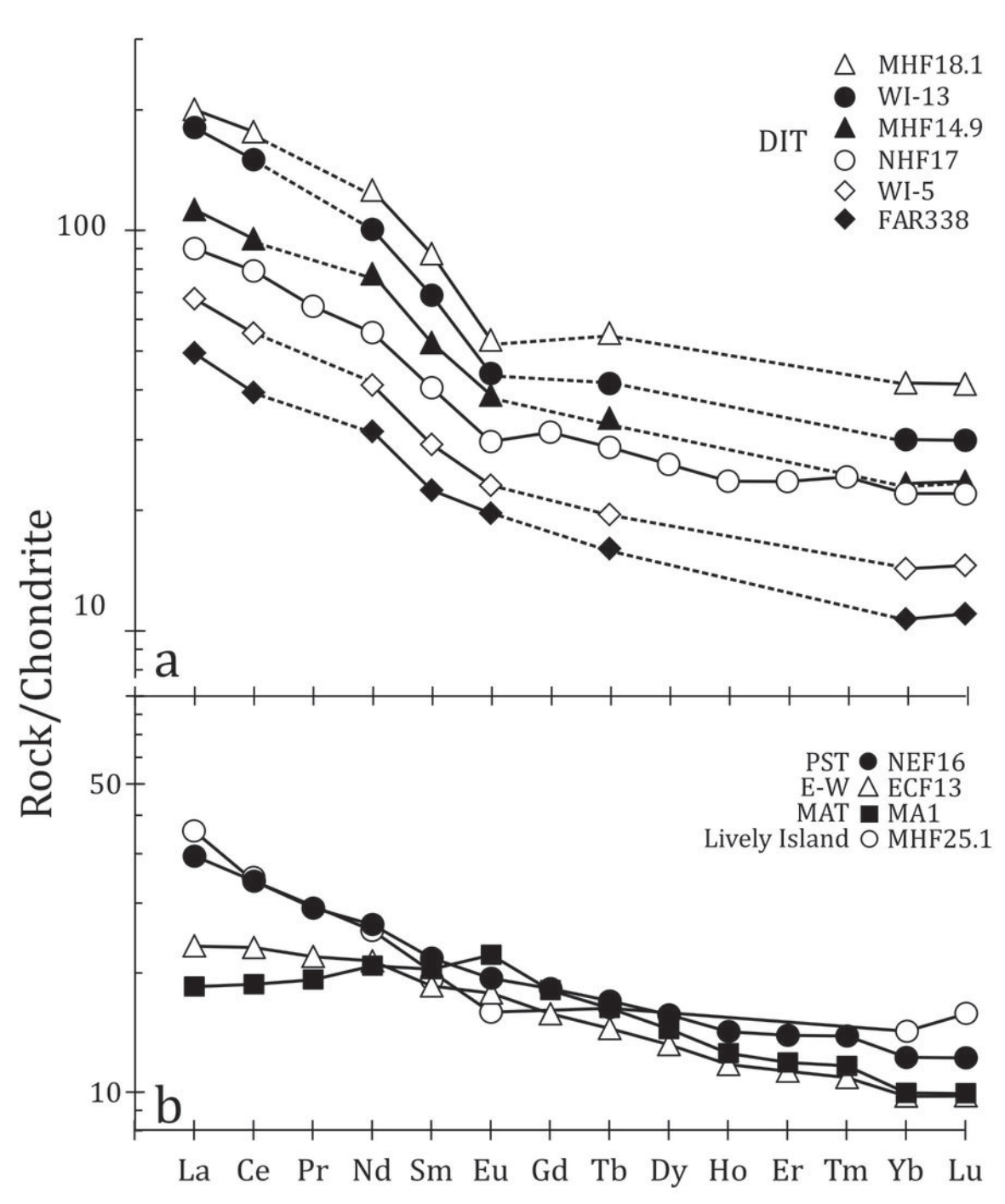
Rock/Chondrite
100
10
a
DIT
MHF18.1
WI-13
MHF14.9
NHF17
WI-5
FAR338
50
10
b
PST NEF16
E-W ECF13
MAT MA1
Lively Island MHF25.1
La Ce Pr Nd Sm Eu Gd Tb Dy Ho Er Tm Yb Lu

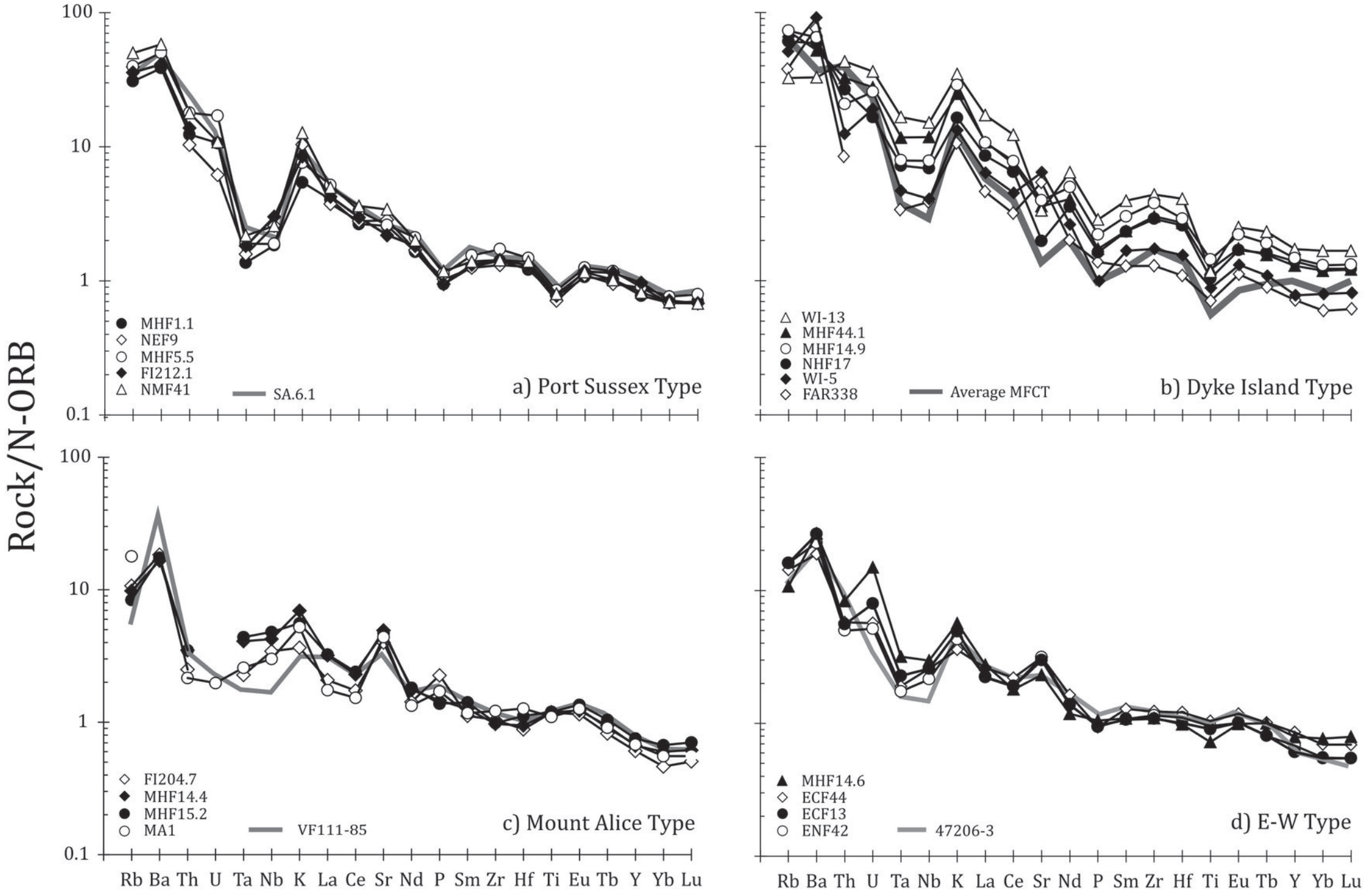
Rock/N-ORB
100
10
1
0.1
MHF1.1
NEF9
MHF5.5
FI212.1
NMF41
SA.6.1
a) Port Sussex Type
WI-13
MHF44.1
MHF14.9
NHF17
WI-5
FAR338
Average MFCT
b) Dyke Island Type
FI204.7
MHF14.4
MHF15.2
MA1
VF111-85
c) Mount Alice Type
MHF14.6
ECF44
ECF13
ENF42
47206-3
d) E-W Type
Rb Ba Th U Ta Nb K La Ce Sr Nd P Sm Zr Hf Ti Eu Tb Y Yb Lu

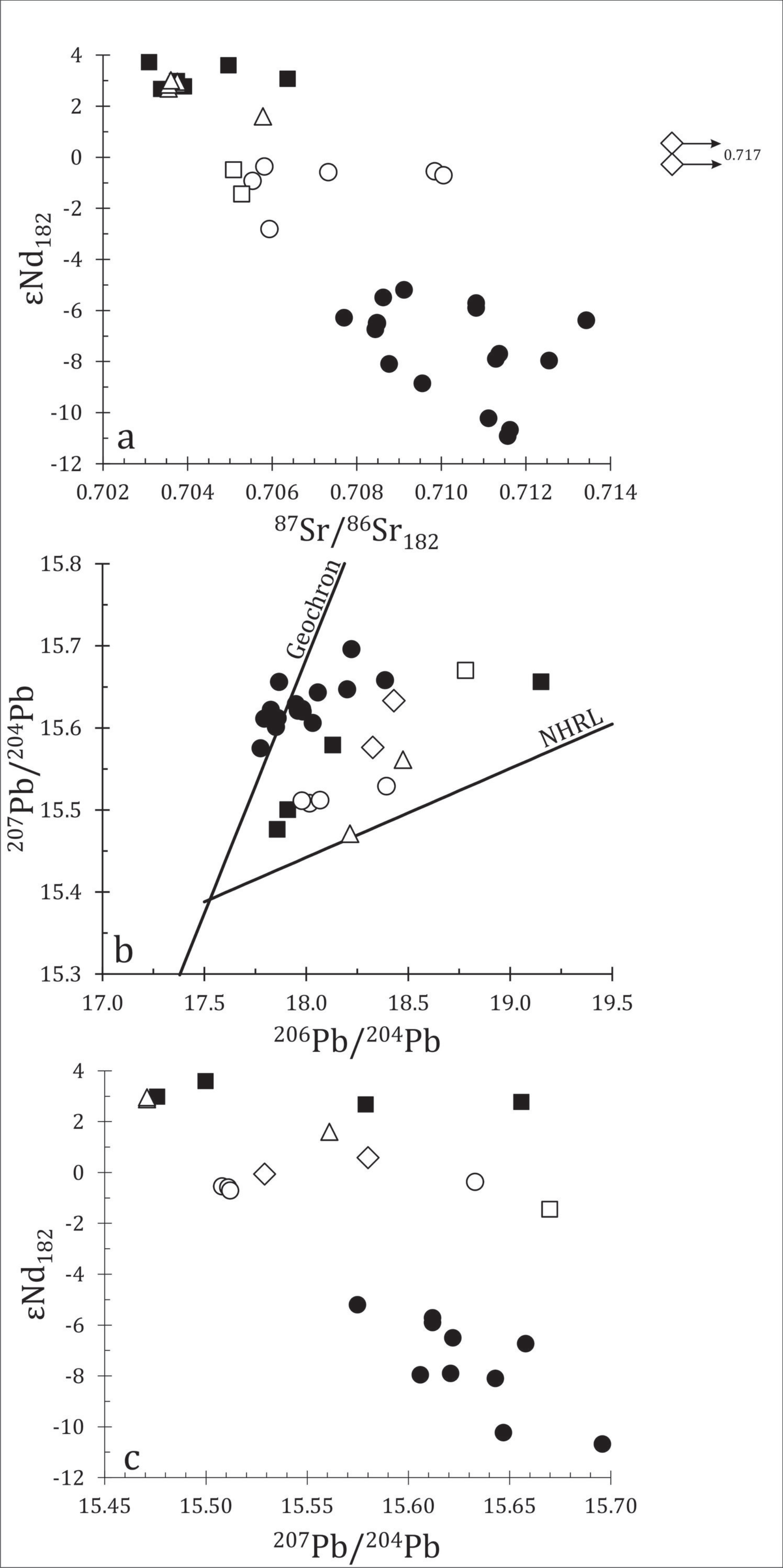
4
2
0
-2
-4
-6
-8
-10
-12
εNd182
a
0.702
0.704
0.706
0.708
0.710
0.712
0.714
87Sr/86Sr182
0.717
15.8
15.7
15.6
15.5
15.4
15.3
207Pb/204Pb
Geochron
NHRL
b
17.0
17.5
18.0
18.5
19.0
19.5
206Pb/204Pb
4
2
0
-2
-4
-6
-8
-10
-12
εNd182
c
15.45
15.50
15.55
15.60
15.65
15.70
207Pb/204Pb

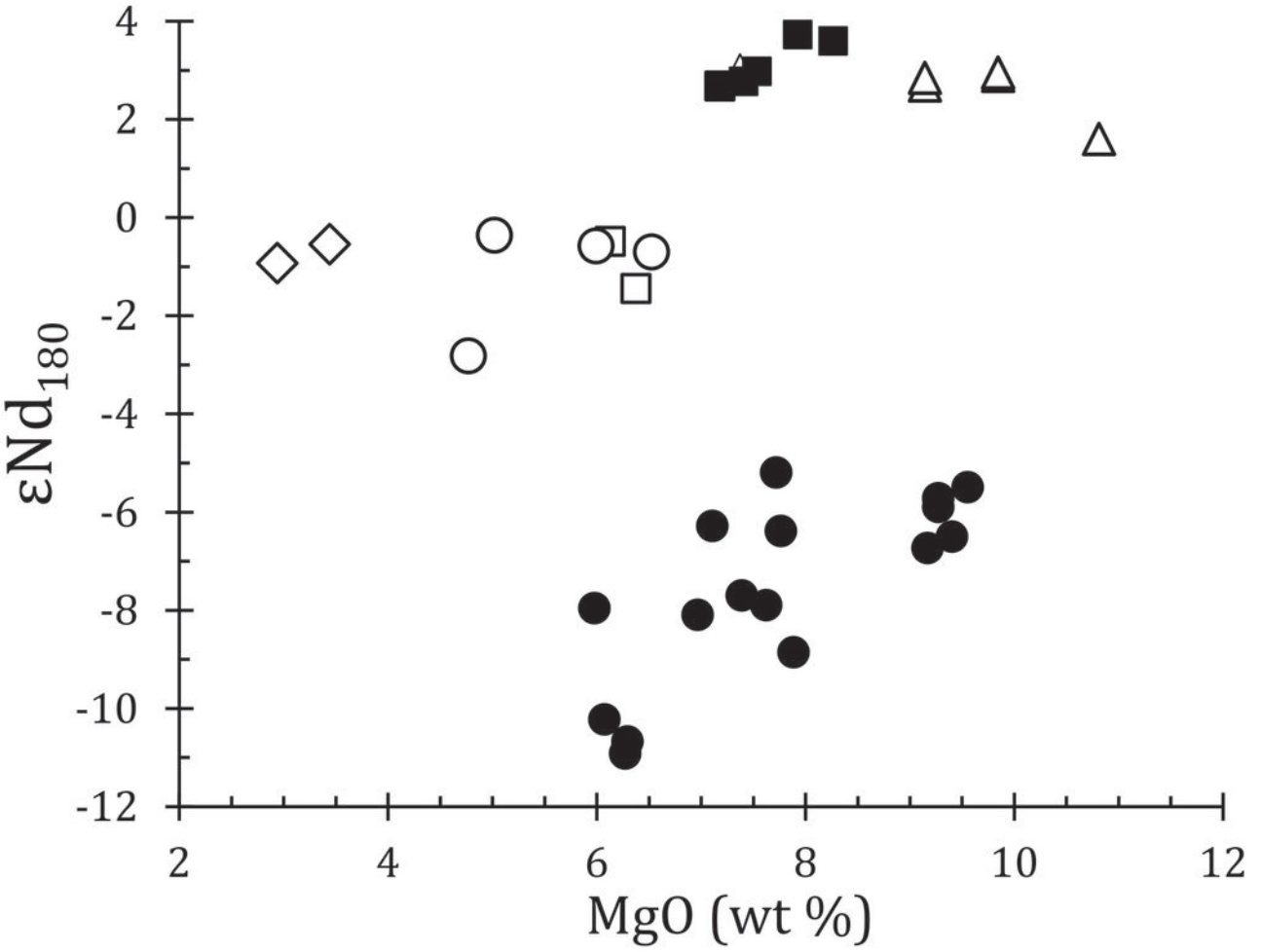
4
2
0
-2
-4
-6
-8
-10
-12
εNd180
2
4
6
8
10
12
MgO (wt %)

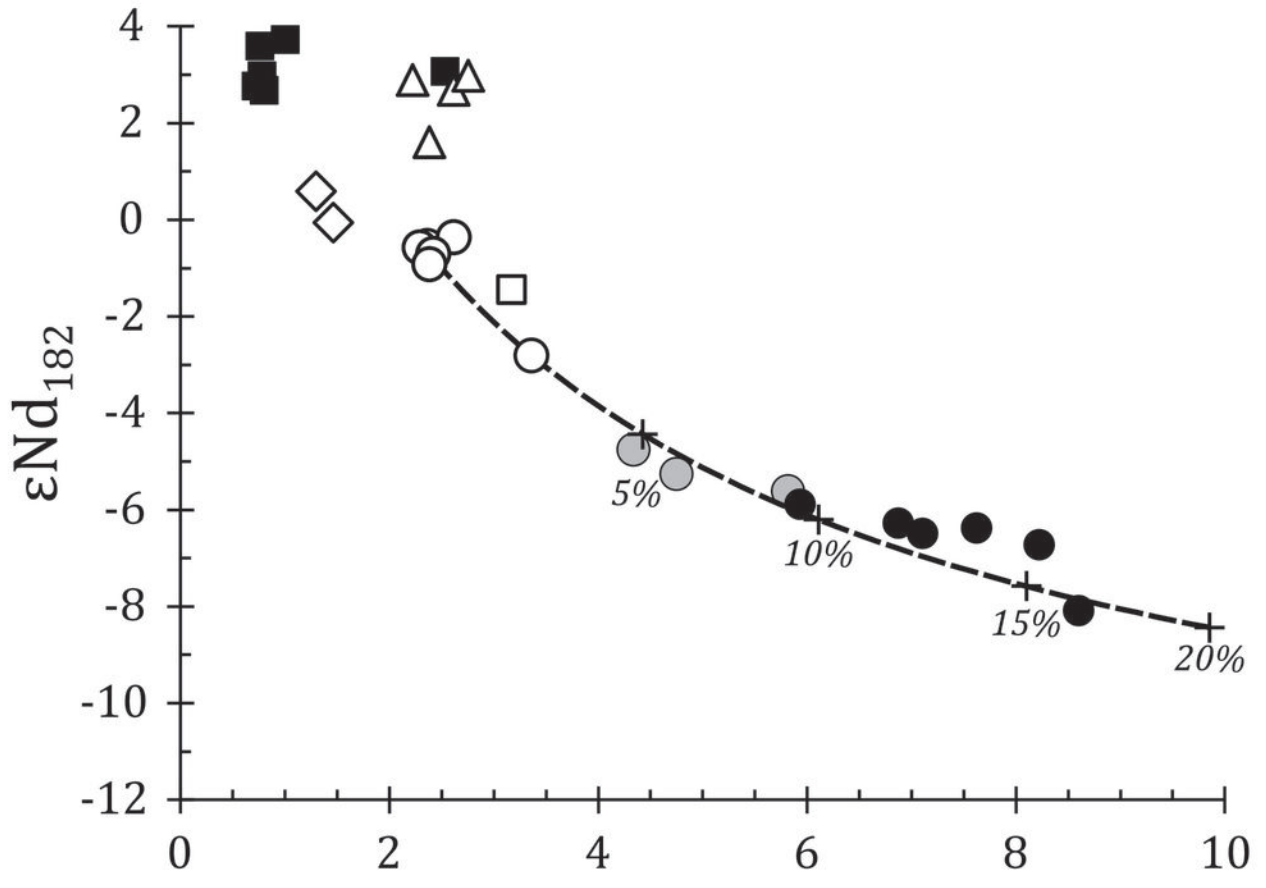
4
2
0
-2
-4
-6
-8
-10
-12
εNd182
5%
10%
15%
20%
0
2
4
6
8
10
Th/Ta

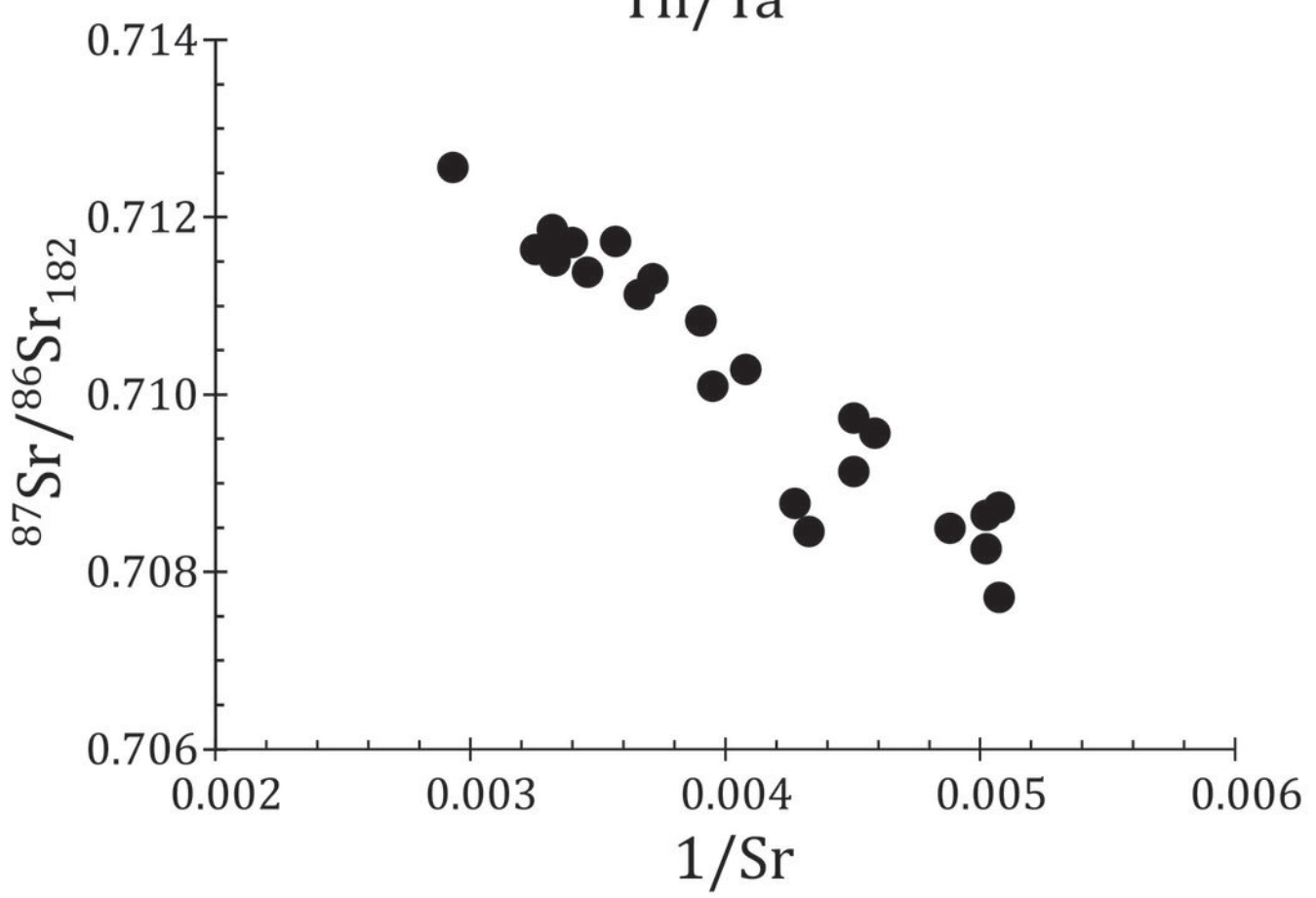
0.714
0.712
0.710
0.708
0.706
87Sr/86Sr182
0.002
0.003
0.004
0.005
0.006
1/Sr

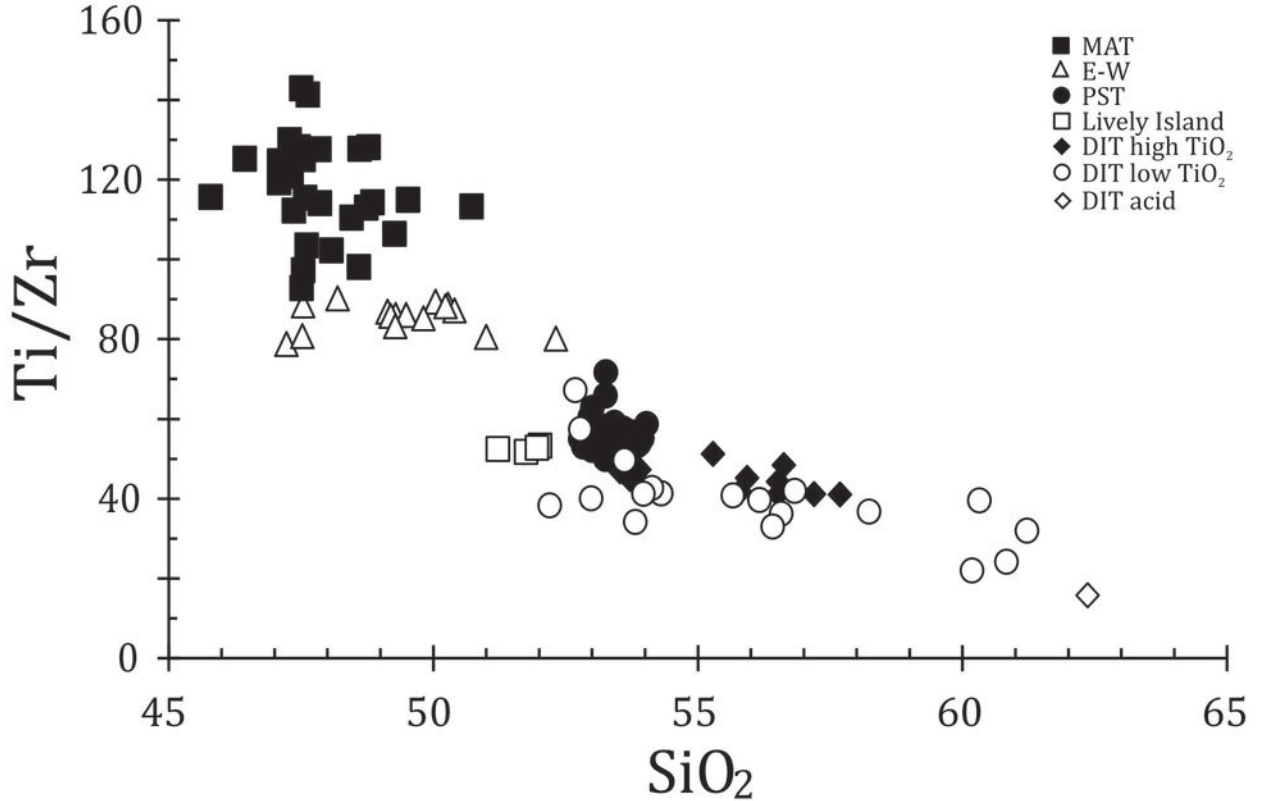
160
120
80
40
0
Ti/Zr
45
50
55
60
65
SiO2
MAT
E-W
PST
Lively Island
DIT high TiO2
DIT low TiO2
DIT acid

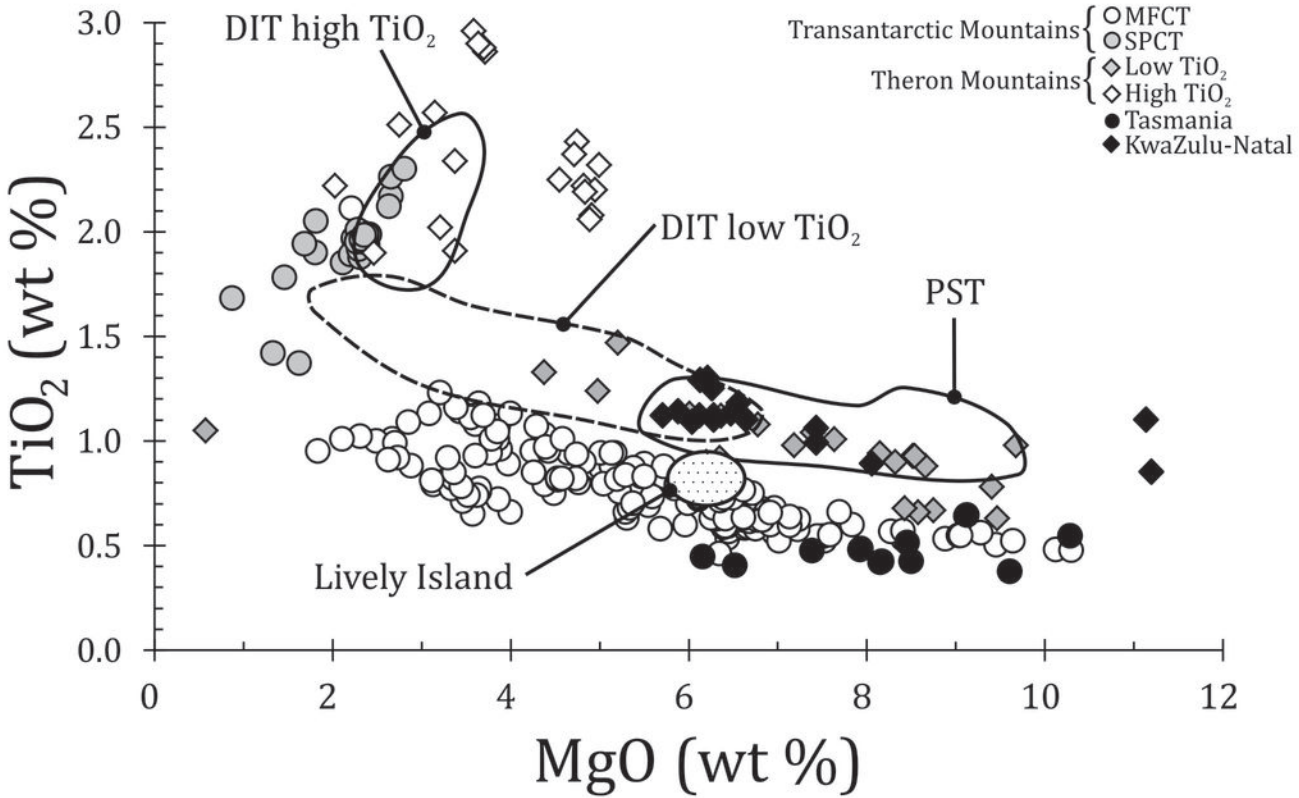
DIT high TiO2
DIT low TiO2
PST
Lively Island
Transantarctic Mountains
MFCT
SPCT
Theron Mountains
Low TiO2
High TiO2
Tasmania
KwaZulu-Natal
TiO2 (wt %)
MgO (wt %)
3.0
2.5
2.0
1.5
1.0
0.5
0.0
0
2
4
6
8
10
12

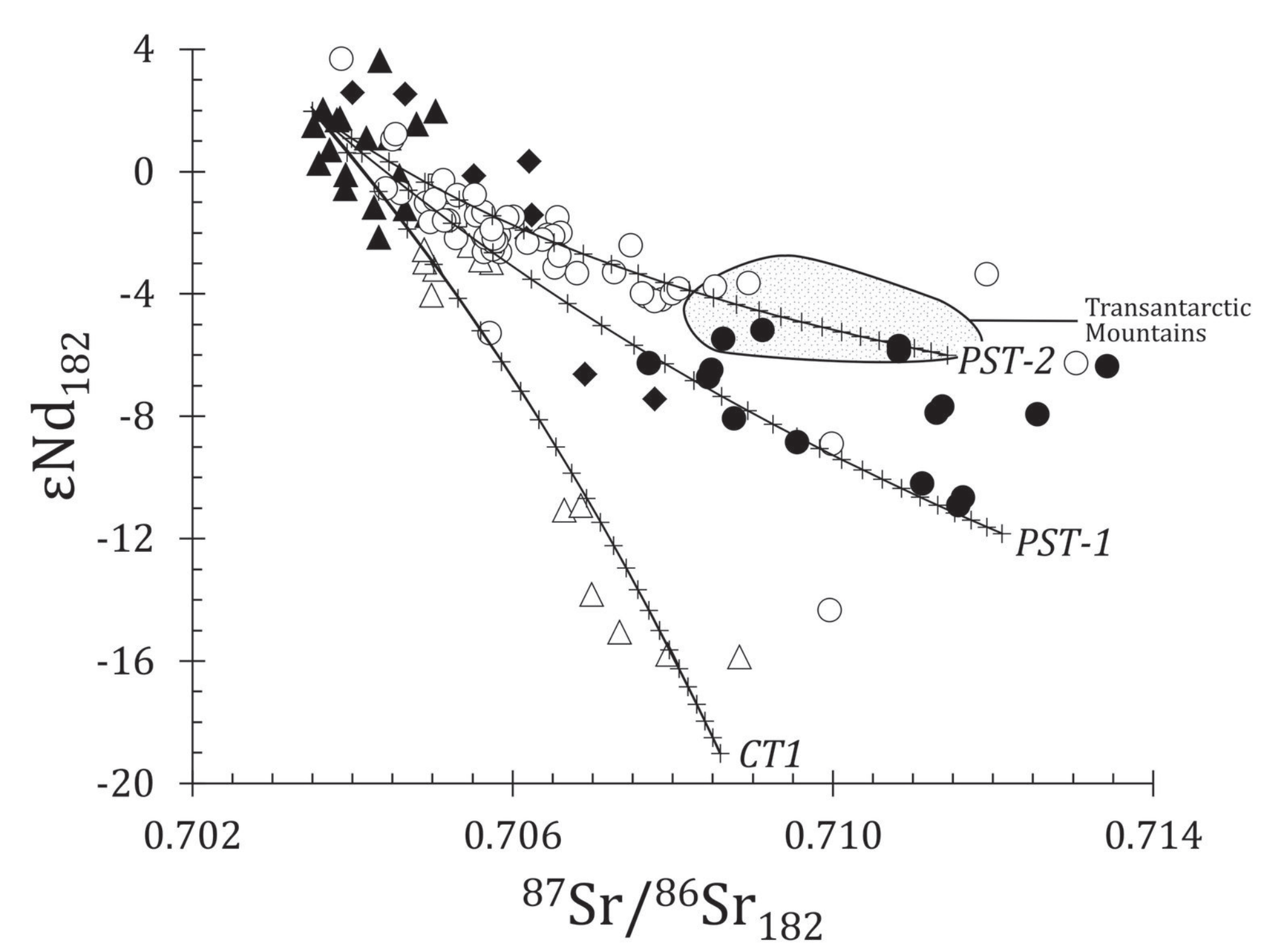
4
0
-4
-8
-12
-16
-20
εNd182
0.702
0.706
0.710
0.714
87Sr/86Sr182
Transantarctic
Mountains
PST-2
PST-1
CT1

a

CaO (weight %)

12
10
8
6
4

5
10
15

peridotite
pyroxenite
augite
B70-AVL
augite+plag+ol
orthopyroxene
olivine
NEF9

MgO (weight %)

b

Cr (ppm)

800
600
400
200
0

45
50
55
60

Mt Shasta Mg-andesite

SiO_2 (weight %)

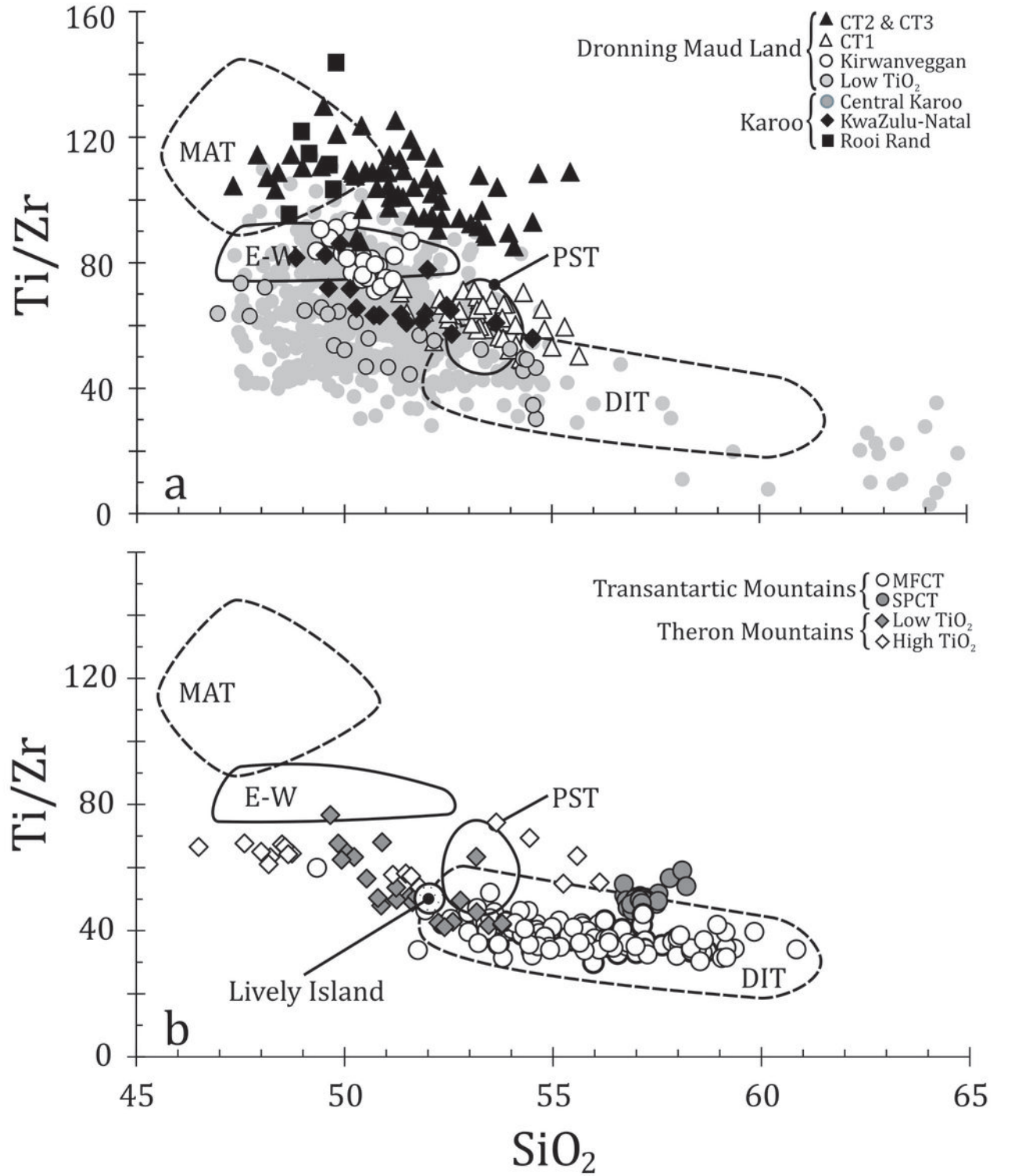
Dronning Maud Land
CT2 & CT3
CT1
Kirwanveggan
Low TiO2
Karoo
Central Karoo
KwaZulu-Natal
Rooi Rand
MAT
E-W
PST
DIT
a
Ti/Zr
160
120
80
40
0
Transantartic Mountains
MFCT
SPCT
Theron Mountains
Low TiO2
High TiO2
MAT
E-W
PST
DIT
Lively Island
b
Ti/Zr
120
80
40
0
45
50
55
60
65
SiO2

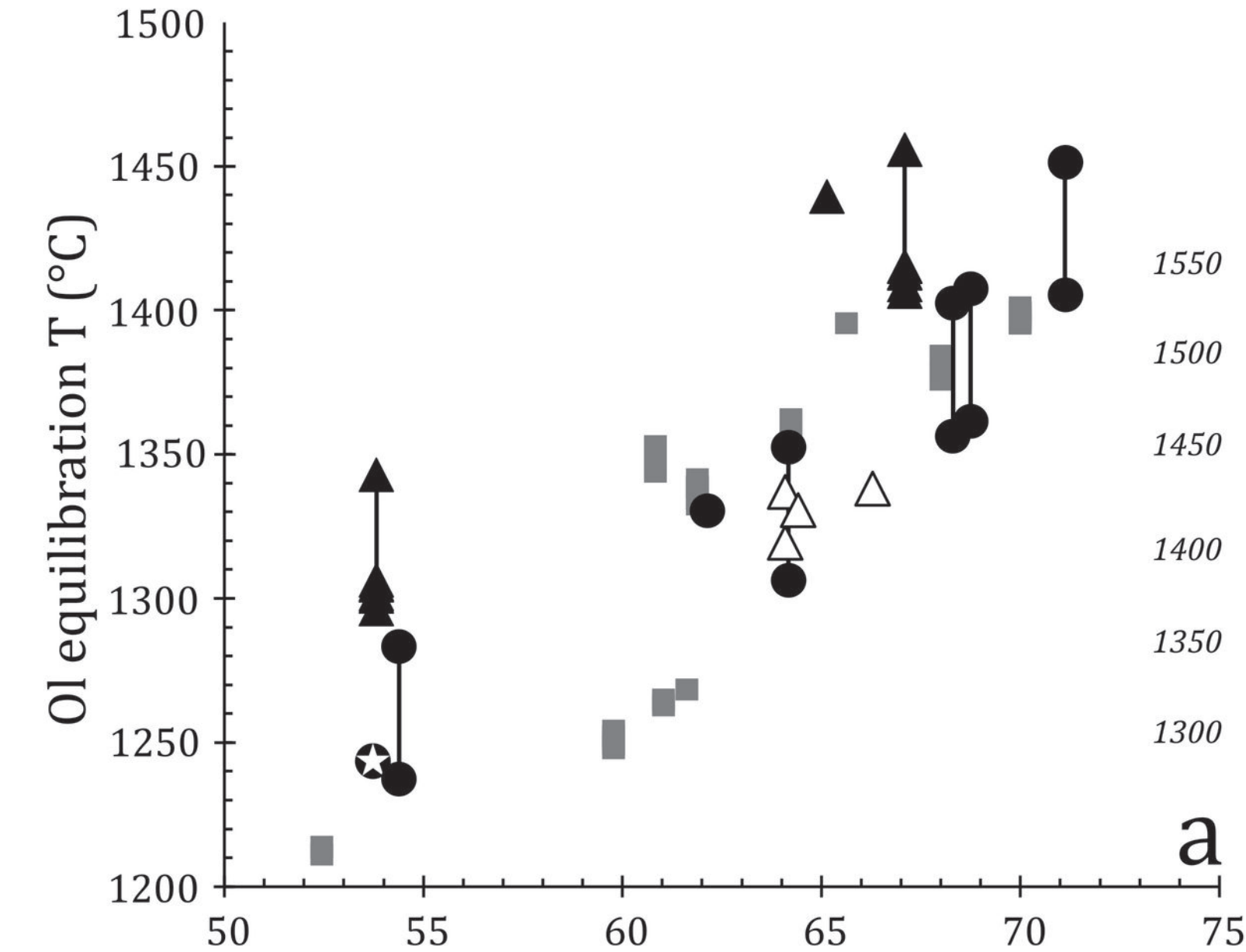
Ol equilibration T (°C)
1500
1450
1400
1350
1300
1250
1200
50
55
60
65
70
75
1550
1500
1450
1400
1350
1300
a

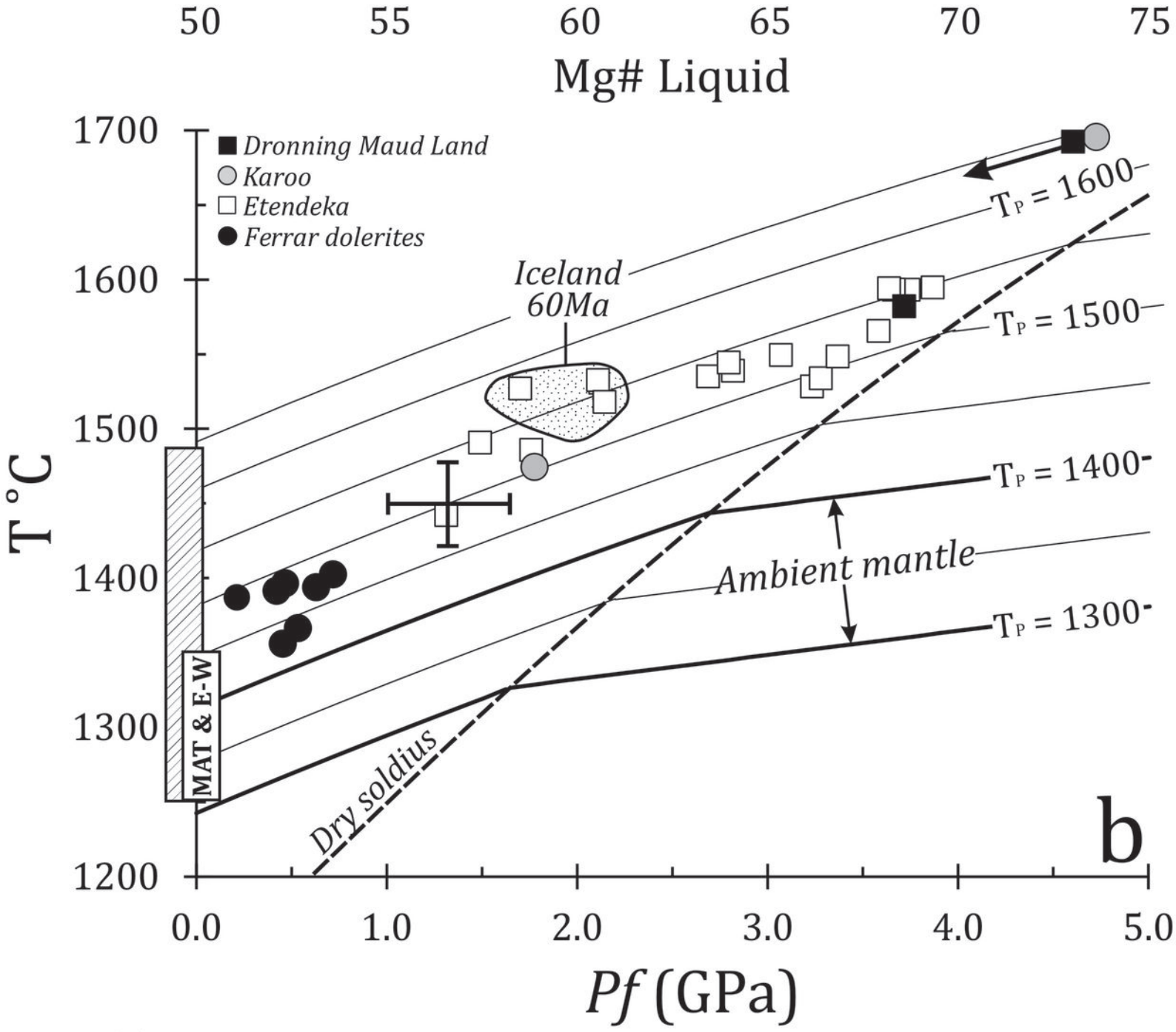
Mg# Liquid
T °C
Pf (GPa)
Dronning Maud Land
Karoo
Etendeka
Ferrar dolerites
Iceland
60Ma
MAT & E-W
Dry soldius
Ambient mantle
TP = 1600
TP = 1500
TP = 1400
TP = 1300
1700
1600
1500
1400
1300
1200
0.0
1.0
2.0
3.0
4.0
5.0
b

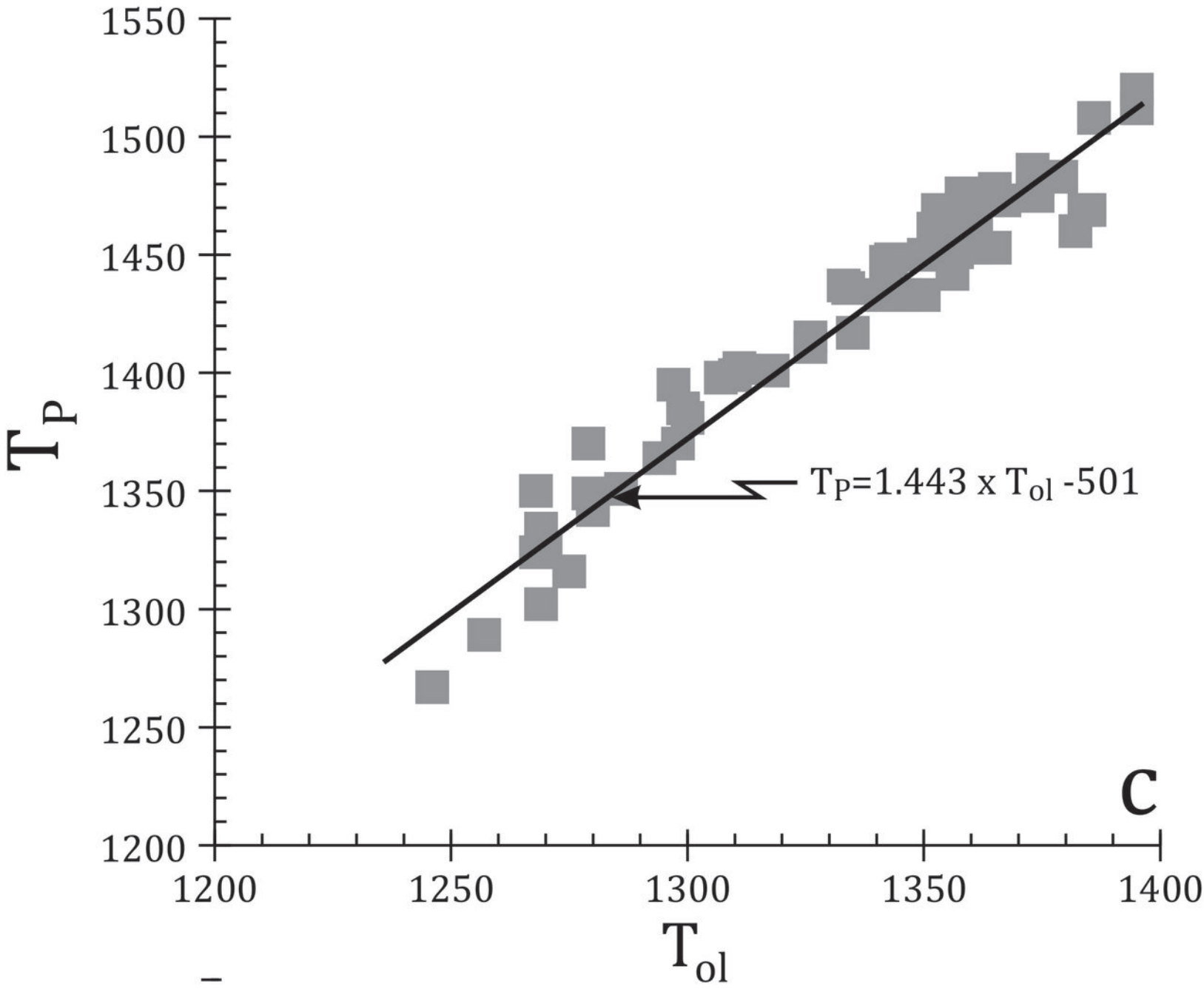
TP
Tol
TP=1.443 x Tol -501
1550
1500
1450
1400
1350
1300
1250
1200
1200
1250
1300
1350
1400
c

Sample	1187-1	#1503	NEF9	NMF41	MHF1.1	MHF5.5	ECF13	ECF42	ECF44	MHF14.6
Type	PST	PST	PST	PST	PST	PST	EW	EW	EW	EW
SiO_2	52.67	53.20	52.41	53.59	53.49	53.01	49.49	49.82	50.40	47.02
TiO_2	0.97	1.02	0.89	1.02	0.99	1.07	1.15	1.21	1.32	0.92
Al_2O_3	14.00	12.90	15.69	14.87	13.15	13.90	14.30	14.47	15.22	14.79
Fe_2O_3	11.94	11.90	11.50	11.25	11.29	12.03	11.91	11.99	11.85	12.54
MnO	0.14	0.14	0.13	0.17	0.13	0.16	0.17	0.18	0.02	0.19
MgO	7.74	9.43	5.96	6.29	9.15	6.93	9.85	9.14	7.38	10.77
CaO	8.63	8.79	9.35	9.24	8.94	9.18	10.20	10.20	10.87	10.49
K_2O	2.45	1.90	2.61	2.52	2.10	2.52	2.47	2.58	2.57	2.33
P_2O_5	0.98	0.46	0.77	0.92	0.40	0.55	0.36	0.31	0.26	0.41
Na_2O	0.18	0.16	0.16	0.14	0.11	0.13	0.11	0.11	0.11	0.11
TOTAL	99.70	99.90			99.75	99.48				99.57
Loss	1.50	0.50			1.26	2.62				2.20
Rb	33.1	14.2	22	28	17	22	9	9	8	6
Sr	533	205	256	307	232	234	269	282	283	208
Nb	5.8	4.9	6	6	4.3	4.4	6	5	6	6.9
Zr	110	93	97	106	104	113	80	85	91	81
Y	23.9	23.1	25	23	22	25.1	17	19	24	22.1
Cr	352	625	589	223	577	255	707	449	310	458
Ni	100	170	133	75	146	91	236	174	113	254
Ba	nd	nd	1235	365	250	316	167	144	126	208
La	11.6	9.3	9.35	12.42	10.10	12.90	5.54	5.60	6.55	6.9
Ce	25.1	20.1	20.87	27.19	19.90	24.90	14.19	14.29	16.48	13.5
Pr			2.77	3.44			2.09	2.10	2.45	
Nd	14.7	12.3	12.37	14.64	12.00	15.3	10.01	10.16	11.95	8.6
Sm	3.58	3.15	3.29	3.68	3.34	4.06	2.80	2.84	3.37	2.87
Eu	1.22	1.05	1.12	1.19	1.09	1.28	1.03	1.03	1.20	1.01
Gd			3.76	4.16			3.25	3.29	4.10	
Tb	0.72	0.63	0.64	0.68	0.77	0.79	0.54	0.54	0.68	0.67
Dy			3.98	4.20			3.35	3.35	4.42	
Ho			0.80	0.83			0.66	0.67	0.85	
Er			2.30	2.37			1.87	1.90	2.41	
Tm			0.35	0.36			0.28	0.28	0.36	
Yb	2.14	1.93	2.08	2.12	2.09	2.33	1.66	1.68	2.11	2.34
Lu	0.33	0.28	0.31	0.31	0.32	0.36	0.25	0.25	0.31	0.36
Th	1.83	1.35	1.24	2.14	1.48	2.15	0.67	0.60	0.69	1.0
U	0.80	0.50	0.29	0.51	0.5	0.8	0.37	0.24	0.27	0.7
Ta	0.24	0.19	0.21	0.29	0.18	0.25	0.30	0.23	0.25	0.42
Hf	2.73	2.33	2.6	2.86	2.49	3.03	2.05	2.27	2.48	2.01
Pb			5.55	4.93			2.19	2.65	2.65	
Cs	0.42	0.29			2.24	0.74				0.3
Co	43.30	47.30			50.8	42.9				61.4
Sc	25.70	26.60			27.8	28.2				35
$^{87}Sr/^{86}Sr$	0.71448	0.70900			0.70900	0.70948				0.70600
± 2SE	±1	± 2			± 18	± 17				±2
$^{87}Sr/^{86}Sr_{182}$	0.71343	0.70848	0.71083		0.70845	0.70877	0.70579	0.70376	0.70355	0.70578
$^{143}Nd/^{144}Nd$	0.512252	0.512255			0.512259	0.512181				0.512726
± 2SE	±7	±5			± 6	± 6				±7
$^{143}Nd/^{144}Nd_{182}$	0.512069	0.512063	0.512367		0.51205	0.511981	0.512561	0.512551	0.512565	0.512475
εNd_{182}	-6.4	-6.5	-5.7		-6.7	-8.1	2.9	2.7	3.0	1.6
$^{206}Pb/^{204}Pb$		17.826±11	17.86		18.394 ±8	18.057± 7		18.21		18.474±7
$^{207}Pb/^{204}Pb$		15.622 ±8	15.61		15.658± 8	15.643 ±8		15.47		15.561±8
$^{208}Pb/^{204}Pb$		38.044±19	37.97		38.143±20	38.246±16		37.58		38.111±15
Sample	1187-1	#1503	NEF9	NMF41	MHF1.1	MHF5.5	ECF13	ECF42	ECF44	MHF14.6

Sample	MHF25.1	FAR338	WI-5	MHF18.3	NHF17	MHF14.9	MHF44.1	WI-3	MHF18.1	MHF41.3
Type	Lively	DIT	DIT	DIT	DIT	DIT	DIT Acid	DIT Acid	DIT Acid	DIT Acid
SiO_2	51.76	52.41	52.44	53.24	53.97	56.06	55.49	60.88	64.11	68.92
TiO_2	0.82	0.89	1.10	1.30	1.32	1.81	1.54	1.63	1.51	0.71
Al_2O_3	15.94	15.69	19.53	15.01	13.27	14.30	15.28	15.24	15.96	15.03
Fe_2O_3	10.33	11.5	8.66	12.05	13.88	12.28	12.31	9.19	10.61	6.57
MnO	0.13	0.13	0.12	0.12	0.22	0.18	0.22	0.12	0.06	0.10
MgO	6.38	5.96	6.54	4.99	4.77	2.93	3.48	1.96	1.67	0.60
CaO	11.27	9.35	7.73	8.56	8.68	5.22	5.63	3.01	0.75	0.40
K_2O	2.46	2.61	2.92	3.21	2.52	4.10	3.76	5.74	3.25	3.51
P_2O_5	0.73	0.77	0.22	0.66	1.18	2.06	1.78	1.10	0.75	3.29
Na_2O	0.17	0.16	0.11	0.17	0.19	0.25	0.20	0.59	0.69	0.21
TOTAL	99.63	99.49	99.36	99.30		99.20	99.69	99.45	99.36	99.34
Loss	1.88	2.10	3.28	3.64		4.12	1.56	2.81	3.30	3.44
Rb	10.9	21.7	29	17.6	34	40.8	40	18.2	20.5	59.6
Sr	231	493.3	582	367	178	358	324	302	1204	715
Nb	10.3	9.1	9.5	12.0	16	18.2	27.4	35.2	74.4	72
Zr	93	96	115	158	192	267	226	309	502	620
Y	21.4	20.0	21.8	30.0	39	41.1	36.2	48.2	85.5	64.8
Cr	172	43	44	71	21	31	11	15	13	19
Ni	63	-	7	95	10	20	6	2.0	8	2.0
Ba	205	494	153	199	371	1409	528	207	2939	862
La	10.8	11.7	16.0	15.7	21.36	26.7	27.0	42.8	47.5	68.9
Ce	21.3	24.1	33.9	32.6	48.50	58.3	55.6	91.9	108	140.0
Pr					6.14					
Nd	11.9	14.7	19.2	20.5	25.93	36.4	29.7	47.0	58.9	69.3
Sm	2.9	3.39	4.41	5.32	6.12	7.92	6.18	10.4	13.2	13.60
Eu	0.92	1.14	1.34	1.63	1.72	2.25	1.77	2.55	3.09	3.41
Gd					6.46					
Tb	0.61	0.60	0.73	0.94	1.07	1.27	1.04	1.55	2.07	2.06
Dy					6.62					
Ho					1.34					
Er					3.91					
Tm					0.62					
Yb	2.41	1.82	2.43	2.81	3.74	3.97	3.62	5.11	7.07	7.47
Lu	0.4	0.28	0.37	0.44	0.0.56	0.60	0.55	0.76	1.05	1.11
Th	1.68	1.03	1.50	1.49	3.19	2.48	3.90	5.17	5.6	6.54
U	0.8		0.90	0.9	0.77	1.20	1.30	1.70	2.2	2.10
Ta	0.53	0.45	0.62	0.57	0.95	1.04	1.54	2.19	4.32	4.47
Hf	2.32	2.24	3.18	3.78	5.29	5.94	5.53	8.35	11.7	13.80
Pb					13.83					
Cs	0.47		0.28	0.4		0.56	0.38	0.20	0.3	0.20
Co	39.3	21.5	23.20	50.6		35.00	29.4	16.70	12.5	7.40
Sc	37.4	17.1	18.80	15.8		24.70	23.7	18.40	16.3	13.30
$^{87}Sr/^{86}Sr$	0.70564	0.70771±1	0.71042	0.70618		0.70730	0.70730	0.71029	0.71720	0.71745
± 2SE	±15	1	±6	±17		± 17	± 17	± 23	±17	±14
$^{87}Sr/^{86}Sr_{182}$	0.70510	0.70733	0.71004	0.70581	0.70594	0.70554	0.70637	0.70983	0.71716	0.71714
$^{143}Nd/^{144}Nd$	0.512505	0.512540±	0.512533 ±8	0.512572		0.512561	0.512561	0.512535	0.512595	0.512542
± 2SE	±8	9		±5		± 6	± 6	± 7	±7	±7
$^{143}Nd/^{144}Nd_{182}$	0.512322	0.512374	0.51236	0.512377	0.512259	0.512349	0.512405	0.512369	0.512427	0.512398
εNd_{182}	-1.5	-0.6	-0.7	-0.4	-2.8	-0.9	3.1	-0.6	0.6	-0.1
$^{206}Pb/^{204}Pb$	18.781± 9	17.980±9	18.067±9	18.430±8				18.016±10	18.326±8	18.393±6
$^{207}Pb/^{204}Pb$	15.670±9	15.510±8	15.512±8	15.633±7				15.508±10	15.576±8	15.529±6
$^{208}Pb/^{204}Pb$	38.300±23	37.361±18	37.425±12	37.944±2				37.492±26	37.880±20	37.583±12

Sample	MHF15.2	MHF14.4	MHF15.1	MA1
Type	MAT	MAT	MAT	MAT
SiO_2	45.92	47.40	48.56	47.51
TiO_2	1.81	1.52	1.71	1.39
Al_2O_3	15.70	16.39	16.71	16.45
Fe_2O_3	13.60	13.23	12.52	12.91
MnO	0.16	0.17	0.21	0.20
MgO	8.00	7.51	7.15	8.27
CaO	10.59	10.65	9.80	10.05
K_2O	2.59	2.53	2.53	2.65
P_2O_5	0.30	0.05	0.17	0.38
Na_2O	0.20	0.17	0.19	0.20
TOTAL	98.87	99.63	99.56	
Loss	1.5	1.90	2.25	
Rb	4.7	5.5	2.0	10
Sr	424	444	381	396
Nb	11.2	9.9	10.7	7
Zr	80	79	80	90
Y	21.1	18.6	18.2	19
Cr	89	78	95	89
Ni	119	102	121	116
Ba	110	105	103	827
La	8.1	8.0	7.9	4.37
Ce	18.0	17.2	18.3	11.45
Pr				1.83
Nd	13.3	12.8	13.8	9.73
Sm	3.72	3.32	3.78	3.08
Eu	1.38	1.25	1.42	1.29
Gd				3.72
Tb	0.7	0.63	0.72	0.61
Dy				3.66
Ho				0.71
Er				1.97
Tm				0.30
Yb	2.05	1.83	2.04	1.69
Lu	0.32	0.28	0.33	0.23
Th	0.42	0.42	0.48	0.26
U				0.09
Ta	0.58	0.54	0.6	0.3
Hf	2.28	1.94	2.26	2.60
Pb				1.07
Cs	0.3	0.35	0.2	
Co	48.2	42.60	49.3	
Sc	28.9	25.40	28.6	
$^{87}Sr/^{86}Sr$	0.70400	0.70385±17	0.70342	
± 2SE	±14		±15	
$^{87}Sr/^{86}Sr_{182}$	0.70392	0.70375	0.70338	0.70497
$^{143}Nd/^{144}Nd$	0.512747	0.512743	0.512738	
± 2SE	±6	±17	±6	
$^{143}Nd/^{144}Nd_{182}$	0.512537	0.512548	0.512532	0.512588
εNd_{182}	2.8	3.0	2.7	3.6
$^{206}Pb/^{204}Pb$	19.152±6	17.858±7	18.131±7	17.91
$^{207}Pb/^{204}Pb$	15.656±5	15.476±6	15.579±7	15.50
$^{208}Pb/^{204}Pb$	38.464±13	37.425±18	37.762±16	37.57

Table 1. Whole-rock major and trace element and isotopic compositions of Falkland Islands intrusions used in this study. Major elements and isotopic compositions for sample numbers starting with EC, NE, NH, NM and MA are from Mitchell *et al.* (1999) with addition trace elements from this study. See supplementary materials for analytical methods.

Table 2. Geochemical, mineralogical and petrographical characteristics of the different groups of Falkland Islands intrusions.

Type	Type locality	Mitchell[1]	Stone[2]	Petrographic features	Mineralogy	Subgroup	Mg#	SiO_2	TiO_2	Ti/Zr	Zr/Y	$^{87}Sr/^{86}Sr_{182}$	εNd_{182}
Port Sussex Creek (PST)	Port Sussex 51º40'15" S 58º58'41" W	N-S	NE-SW	Coarse-grained dolerite	Pig ± Opx + Aug Rare Ol + Di	none	48-58	52-54	0.9-1.2	50-70	3.6-5.3	0.7077 -0.7134	-5.5 to -10.9
E-W	Fox Bay West 51º57'02" S 60º05'21" W	E-W	E-W	Coarse-grained olivine dolerite	Ol + Plag ± Aug	none	42-64	47-54	1.0-1.9	77-90	3.2-4.8	0.7036-0.7058	-0.4 to +3.0
Lively Island (LI)	Lively Island 52º00'00" S 58º27'47" W	Lively Island	NE-SW	Coarse-grained with accessory biotite	Ol + Plag + Aug ± rare pigeonite	none	48-52	51-52	0.8-0.9	53	4.0-4.54	0.7053	-0.5 to -1.4
Dyke Island (DIT)	Dyke Island 51º59'33" S 60º52'50" W	Not defined	Radial swarm	Fine-grained aphyric, rarely plagioclase ± augite-phyric	Plag + Aug	Acid	<22	62-75	0.2-1.6	<31	5.0-8.8	0.7055-0.7098	-2.8 to -0.5
						Low TiO_2	27-57	52-61	1.1-1.7	24-67	4.8-7.4		
						High TiO_2	41-51	53-58	>1.80	25-53	6.8-8.4		
Mount Alice (MAT)	Mount Alice 52º09'12" S 60º35'55" W	Mount Alice	Radial swarm	Fine-grained plagioclase ± olivine phyric	Ol + Plag ± Aug	none	44-64	47-50	1.3-1.9	98-142	3.2-5.2	0.7031-0.7039	0.0 to +3.7

1. Groups described by Mitchell *et al*. (1999); 2. Groups defined by Stone *et al.* (2009)

Calculated extract for fractionation of PST and E-W intrusions

	PST			E-W		
	NGF16	MHF5.1	Calc	ECF12	ECF44	Calc
SiO_2	54.01	53.81	53.82	49.69	51.03	50.98
TiO_2	0.94	1.00	1.13	1.05	1.21	1.36
Al_2O_3	13.20	14.97	15.02	13.30	15.21	15.20
FeO	10.60	10.62	10.60	10.51	11.11	11.06
MnO	0.20	0.17	0.18	0.17	0.17	0.21
MgO	9.67	6.78	6.78	11.62	6.71	6.70
CaO	8.81	9.50	9.49	9.81	11.51	11.50
Na_2O	1.96	2.62	2.56	2.29	2.56	2.46
K_2O	0.48	0.42	0.56	0.32	0.39	0.39
P_2O_5	0.12	0.11	0.15	0.11	0.11	0.13
Extract			%			%
Olivine	Fo_{83}		0.0			57.0
Plagioclase	An_{70}		18.9			40.4
Pyroxene	$En_{71}Fs_{19}Wo_9$		74.7			
Pyroxene	$En_{51}Fs_{13}Wo_{33}$		6.4			2.6
Σ residuals^2			0.127			0.038
F			0.79			0.75

Table 4 AFC parameters for the trajectories shown in Fig. 12. R is the ratio of assimilated rock to crystal cumulate. A value appropriate for upper-crustal contamination has been used. F is the total amount of crystallization required to reach the most extreme composition on a particular trajectory. T_{CHUR} is the Chondritic Uniform Reservoir model Nd age for the most extreme composition on a particular trajectory, in Ga.

		AFC parameters								T_{CHUR}
		Sr	**Nd**	**εNd**	**$^{87}Sr/^{86}Sr$**	**D_{Sr}**	**D_{Nd}**	**R**	**F**	**(Ga)**
CT1	Source	50	5	2	0.7035	0.5	0.1	0.40	≤0.2	3.0
	Crust	400	20	-50	0.7120					
PST-1	Source	60	4	2	0.7035	0.5	0.1	0.40	≤0.2	2.2
	Crust	350	40	-20	0.7200					
PST-2	Source	100	5	2	0.7035	0.5	0.1	0.40	≤0.2	1.8
	Crust	350	60	-10	0.7250					